

Original Article

Cite this article: Pérez Luján SB, Boedo FL, Ariza JP, Vujovich GI, Alvarado P, and Kay SM (2021) The Cuyano proto-ocean between the Chilenia and Cuyania terranes: rifting and plume interaction during the Neoproterozoic – early Palaeozoic evolution of the SW Gondwana margin. *Geological Magazine* **158**: 1773–1794. <https://doi.org/10.1017/S0016756821000303>

Received: 17 August 2020

Revised: 19 March 2021

Accepted: 23 March 2021

First published online: 27 April 2021


Keywords:

continental flood basalts; E-MORB; oceanic crust; Iapetus Ocean; Western Argentine Precordillera

***Author for correspondence:**

Sofía B. Pérez Luján, Group de Sismotectónica, Email: sofiap.lujan@unsj-cuim.edu.ar

The Cuyano proto-ocean between the Chilenia and Cuyania terranes: rifting and plume interaction during the Neoproterozoic – early Palaeozoic evolution of the SW Gondwana margin

Sofía B. Pérez Luján^{1,2} , Florencia L. Boedo³, Juan P. Ariza^{2,4}, Graciela I. Vujovich^{3,5}, Patricia Alvarado^{1,6} and Suzanne M. Kay⁷

¹Grupo de Sismotectónica, Centro de Investigaciones de la Geósfera y la Biósfera (CIGEOBIO) - CONICET, San Juan J5402DCS, Argentina; ²Departamento de Geología, Facultad de Ciencias Exactas, Físicas y Naturales - Universidad Nacional de San Juan, San Juan J5402DCS, Argentina; ³CONICET – Universidad de Buenos Aires, Instituto de Estudios Andinos “Don Pablo Groeber” (IDEAN), Buenos Aires C1428EGA, Argentina; ⁴Instituto Geofísico Sismológico Volponi – CONICET, Universidad Nacional de San Juan, San Juan 5407, Argentina; ⁵Servicio Geológico Minero Argentino (SEGEMAR), Instituto de Geología y Recursos Minerales, Buenos Aires B1650KNA, Argentina; ⁶Departamento de Geofísica y Astronomía, Facultad de Ciencias Exactas, Físicas y Naturales - Universidad Nacional de San Juan, San Juan J5402DCS, Argentina and ⁷Department of Earth and Atmospheric Sciences and INSTOC, Cornell University, Ithaca, NY 14853, United States

Abstract

The Precordillera mafic–ultramafic belt (PMUB), located in central-western Argentina, comprises mafic and ultramafic bodies interlayered and/or in tectonic contact with marine siliciclastic units. Whole-rock, mineral geochemistry and Nd–Sr isotope analyses performed in magmatic rocks suggest a relatively different spatial and temporal evolution along the belt. The southern PMUB (south of 32° S) evolved as an intra-continental rifted margin with an enriched mid-ocean-ridge basalt (E-MORB) tholeiitic to alkaline magmatism, to a proto-ocean basin (the Cuyano proto-ocean) with tholeiitic normal-MORB geochemical signature. Based on neodymium model ages (T_{DM}), the magmatic activity started during the late Neoproterozoic Era and continued into the early Palaeozoic Era. Instead, the northern PMUB (28–32° S) evolved as an intra-continental rifted margin with dominant tholeiitic E-MORB to continental flood basalt (CFB) magmatism during the early Palaeozoic Era. ϵ_{Nd} values (+3.4 to +8.4), rare earth element trends and high-field-strength element systematics, together with an estimated potential mantle temperature of *c.* 50–100°C above ambient mantle, suggest the PMUB magmatism derived from an enriched mantle source related to the effect of a rising plume linked to the Iapetus Ocean opening. In particular, T_{DM} estimations of 600–550 Ma agree with reported magmatism in central to southern Appalachians. The magmatism in the PMUB, and those registered in the Neoproterozoic Catocin Formation and in the Southern Oklahoma Aulacogen in the conjugated Laurentian margin, seem to be contemporaneous, sharing a similar plume-enriched mantle source. In this context, the E-MORB signature identified along the PMUB can be described as a plume-distal ridge tectonic setting over an extended margin.

1. Introduction

Basalts are important rocks in orogenic settings because they can be related to past sutures between different terranes. However, they can be linked to a wide variety of tectonic settings; geochemistry and isotope geology are therefore powerful tools to obtain information about the tectonic origin of basaltic rocks (e.g. Pearce, 2008). In particular, subcontinental and sub-oceanic mantle sources can be evaluated in the generation of magmas derived from continental rifting and break-up. Processes of continental rifting initiation can produce continental flood basalts (CFBs) and enriched mid-ocean-ridge basalts (E-MORBs) related to passive and/or active upwelling events in the mantle (e.g. Bosworth *et al.* 2015).

CFBs and E-MORBs studied worldwide are typical tholeiites with low- and high-Ti content, relative high concentration of light rare earth elements (LREEs) and large-ion lithophile elements (LILEs) (De Min *et al.* 2003). Even though MORBs and CFBs derive from partial melting of upwelling mantle, geochemical differences between them are the result of primary mantle composition, depth of partial melting, magmatic processes involved or the interaction with continental crust and/or lithosphere components.

MacDougall (1988) suggests that the generation of CFBs is directly related to a documented hotspot, whereas the generation of E-MORBs is not necessarily linked to hotspots. Pearce (2008)



Fig. 1. (Colour online) Map of central-western Argentina showing the different terranes accreted to the western Gondwana margin during early Palaeozoic time and the Rio de la Plata craton (modified from Ramos *et al.* 1998). Dashed pink lines represent terrane boundaries and the pink area represents the Argentine Precordillera fold-and-thrust belt. Location of the Precordillera mafic-ultramafic belt (PMUB) localities are divided into a northern and a southern sector.

states that this signature characterizes plume-distal ridges together with some incipient oceans and some small basins in long transform segments. Donnelly *et al.* (2004) postulate that E-MORBs can be generated by: (1) low-degree melts that metasomatize the upper mantle to create an enriched source, which later undergoes large extents of melting; or (2) continuous processes of formation and destruction of enriched mantle sources by melting and convective mixing.

E-MORB magmatism is widespread in central-western Argentina, where a mafic-ultramafic belt is exposed over 400 km north-south along the western margin of the Precordillera (Fig. 1). This belt has been traditionally interpreted as the suture zone between the Chilenia and Cuyania terranes, both accreted during early Palaeozoic time to the western Gondwana margin (Ramos *et al.* 1986). Although some geochemical and petrogenetic studies have been carried out on the mafic rocks (Haller & Ramos, 1984; Kay *et al.* 1984; Boedo *et al.* 2013; González-Menéndez *et al.* 2013), many aspects still remain unknown such as precise age, tectonic setting of origin, mantle source composition and their implications on how this sector of the Precordillera has evolved.

Borrello (1969) and Haller & Ramos (1984) suggested that the belt belongs to an almost complete and dismembered ophiolite sequence. Based on whole-rock geochemistry, some studies have postulated an oceanic within-plate, plume-related environment, unevolved oceanic rift next to a continental margin and a retro-arc basin as possible geological settings for the Precordillera mafic-ultramafic belt (PMUB) (Cortezzi *et al.* 1982; Kay *et al.* 1984; Cortés & Kay, 1994). Others argue that the gabbros and pillow basalts originated in an evolved continental rift margin with poor crustal contamination (González-Menéndez *et al.* 2013). In this context, Boedo *et al.* (2013) proposed that the whole-rock geochemical imprint of the mafic rocks of the PMUB could be related to a Continental Margin Ophiolite, according to the classification of Dilek & Furnes (2011).

This work includes the geochemical study of mafic and ultramafic rocks exposed in the northern sector of the Western

Argentine Precordillera belt (Rodeo, Alto del Colorado, Sierra del Tigre and Sierra de la Invernada localities; Figs 1, 2). New mineral analyses of pyroxene from the northern (Calingasta area) and southern (Peñasco, Pozos, Cerro Redondo and Cortaderas; Figs 1, 2) sectors are also included. In addition, we report neodymium (Nd)-strontium (Sr) isotope analyses of the same mafic and ultramafic rock samples, providing valuable information to discuss the source of the magmatism and its geotectonic origin. New geochemical analyses are integrated with previously published data of the PMUB. The integrated database is compared with hot-spot-related mafic rocks from southern Laurentia to test for a similar Neoproterozoic – early Palaeozoic evolution of the western Gondwana margin.

2. Geological framework

2.a. The Western Argentine Precordillera

The basement of the Central Andean Cordillera and back-arc region (27–33.5° S) consists of different terranes that were accreted to the western Gondwana margin during the Palaeozoic Era (e.g. Ramos *et al.* 1986) (Fig. 1). In particular, the Argentine Precordillera of central-western Argentina is a Miocene fold-and-thrust belt, located at the front of the Andean Orogen, where lower Palaeozoic rocks belonging to the composite Cuyania terrane (Pie de Palo block + Precordillera) are exposed. Its basement is indirectly known by xenoliths hosted in Neogene volcanic rocks that yield U–Pb zircon ages of 1000–1100 Ma (Leveratto, 1968; Kay *et al.* 1996; Rapela *et al.* 2010).

The lower Palaeozoic stratigraphy of the Precordillera mainly consists of a Cambrian – Lower Ordovician carbonate platform to the east, and Middle–Upper Ordovician marine siliciclastic rocks intercalated with mafic and ultramafic bodies affected by a complex synmetamorphic deformation to the west. Lower Palaeozoic layers are overlain by Silurian–Devonian siliciclastic facies (Haller & Ramos, 1984; Astini *et al.* 1995; Thomas & Astini, 2003).

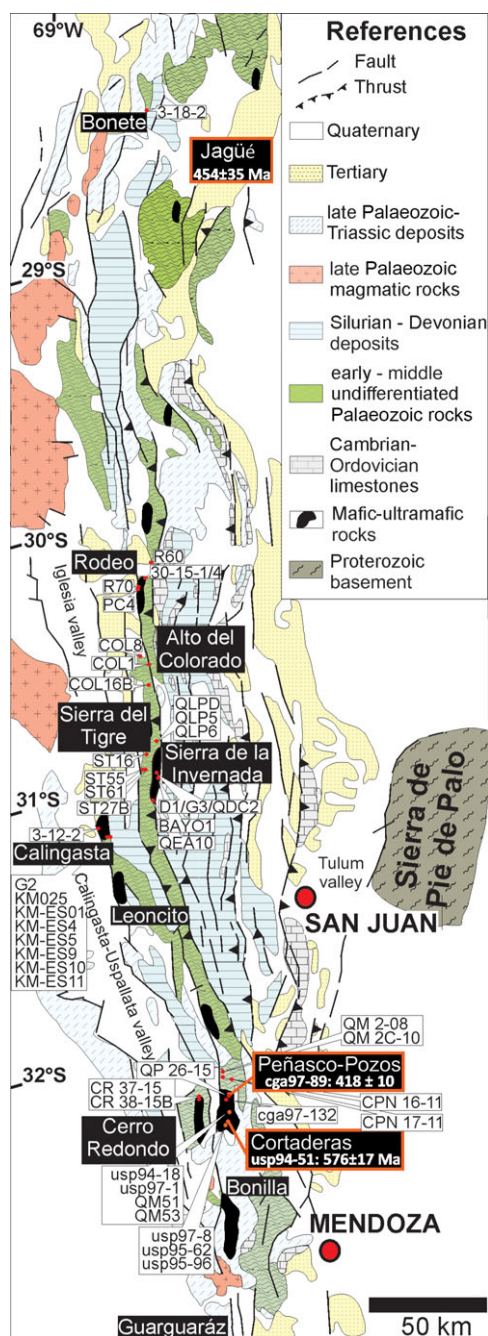


Fig. 2. (Colour online) Geological map of the Argentine Precordillera (modified from Baldis *et al.* 1982). Black named squares show the location of the Precordillera mafic-ultramafic belt areas (see Fig. 1). Black squares with red border indicate U-Pb crystallization ages on zircon (Davis *et al.* 2000; Fauqué & Villar, 2003). Location of studied samples are also shown (Table 1).

The mafic and ultramafic studied bodies, referred to here as the western PMUB, include basaltic pillow lavas, gabbros, diorites and wehrlites that are intruded and/or tectonically juxtaposed in marine siliciclastic metasedimentary successions that occasionally host platform carbonate and siliciclastic olistoliths (Thomas & Astini, 2003). According to lithological aspects and metamorphic grade, the PMUB can be separated into two sectors (Fig. 1). The northern sector (28–32° S) comprises the Jagüé-Bonete (at La Rioja province), Rodeo, Alto del Colorado, Sierra de la Invernada, Sierra del Tigre, Calingasta and Leoncito areas (located in San Juan province). It

comprises basalts and gabbros interbedded with thick siliciclastic successions of Sandbian–Katian–Hirnantian age grouped in the Yerba Loca, Sierra de la Invernada and Alcaparrosa formations (Furque, 1983; Ortega *et al.* 2008). The siliciclastic sequence from the Sierra de la Invernada Formation has been interpreted as turbidites deposited in a storm-dominated shallow-marine shelf (Basilici *et al.* 2005; Gomes *et al.* 2005; Moretti, 2009). The southern sector (32–33° S; Fig. 1) includes the Peñasco, Pozos, Cerro Redondo, Cortaderas and Bonilla localities (all located in Mendoza province). This sector is characterized by serpentinites, ultramafic cumulates, mafic granulites and orthogneisses that are not exposed in the north. Gabbros, basaltic dykes and/or sills, pillow basalts and metahyaloclastite bodies are also interbedded in marine siliciclastic successions (Davis *et al.* 1999; Boedo *et al.* 2013, 2020). Radiometric ages and palaeontological data suggest that sedimentation and basaltic magmatism in a marine basin occurred in this region during late Neoproterozoic – Early Devonian time (Davis *et al.* 2000; Rubinstein & Steemans, 2007; Boedo *et al.* 2020). This sector of the PMUB can be correlated with the Frontal Cordillera mafic-ultramafic belt, exposed S-wards in the Sierra de Guarguaraz, Argentine Frontal Cordillera (Fig. 1). There, serpentinites, metaperidotites, orthoamphibolites, metagabbros, metabasaltic dykes and pillow metabasalts are in contact with marble and schist (López & Gargori, 2004; López de Azarevich *et al.* 2009; Gargiulo *et al.* 2011). The Argentine Frontal Cordillera mafic bodies have an N-MORB to E-MORB chemical signature, and the whole sequence is strongly deformed and metamorphosed. Massonne & Calderón (2008) and Willner *et al.* (2011) estimated a *P-T-t* clockwise metamorphic path in metapelites and metabasites, where high-pressure conditions were followed by decompression with slight heating.

The northern sector of the PMUB exhibits very-low- to low-temperature and pressure metamorphic conditions (0.2–0.3 GPa and 200–350°C; Rubinstein *et al.* 1997; Robinson *et al.* 2005), whereas low- to medium-temperature and high-pressure conditions have affected the southern sector (0.7–0.9 GPa and 345–395°C; Boedo *et al.* 2016). High-temperature and high-pressure conditions have been estimated for mafic granulites exposed in the Peñasco and Cortaderas areas (1.1–1.8 GPa and 650–910°C; Davis *et al.* 1999; Boedo *et al.* 2016). Dating of the low-grade metamorphic event registered in the PMUB and in the Frontal Cordillera belt generally yields a Middle–Late Devonian age (Cucchi, 1971; Davis *et al.* 1999; Willner *et al.* 2011).

Most interpretations agree that the Cuyania terrane rifted away from southern Laurentia (i.e. the Ouachita embayment) during early Cambrian time and drifted across the Iapetus Ocean until it collided against the Gondwana margin during the Late Ordovician Epoch (e.g. Ramos *et al.* 1986; Astini *et al.* 1995; Thomas *et al.* 2012). Alternative models consider a more oblique movement along the Gondwana margin that controlled the accretion of the Pie de Palo and Precordillera blocks (Finney, 2007; Casquet *et al.* 2008).

The PMUB has been interpreted as a dissected ophiolite (Haller & Ramos, 1984) exposed by the collision of the Chilenia terrane against the Gondwana margin (Ramos *et al.* 1986). Davis *et al.* (1999, 2000) have shown that this belt comprises rocks from different tectonic settings such as mid-ocean-ridge and volcanic-arc environments.

2.b. Previous geochronological and geochemical studies of the PMUB

Although there are many studies of the geochemistry of the PMUB, ages of the mafic magmatism are poorly constrained. In the

northern sector, some ages have been indirectly interpreted from basalts interbedded with metasedimentary rocks bearing fossil fauna of Sandbian–Hirnantian age (Ortega *et al.* 2008). A crystallization age of 454 ± 35 Ma (U–Pb on zircon) from basalts is available for the Jagüé–Bonete area (Fig. 2) (Fauqué & Villar, 2003). In addition, estimations from a basic sill for the same locality provided a depleted mantle (DM) Nd model age (T_{DM}) of 510 Ma (Martina *et al.* 2014).

In the southern PMUB sector, Davis *et al.* (2000) obtained two crystallization ages of 576 ± 17 Ma and 418 ± 10 Ma (U–Pb on zircon) on basaltic rocks from the Cortaderas area (Fig. 2), suggesting that the magmatic activity developed from late Neoproterozoic time to the Silurian–Devonian boundary.

Whole-rock geochemistry from basalts and gabbros of the PMUB have an E-MORB signature (Haller & Ramos, 1984; Kay *et al.* 1984; Cortés & Kay, 1994; Boedo *et al.* 2013; González-Menéndez *et al.* 2013) and positive ϵ_{Nd} values that suggest both an oceanic and/or a transitional affinity (extended continental margin) (Cortés & Kay, 1994; Kay *et al.* 2005).

3. Data and methods

This study presents new whole-rock, mineral chemical and Nd and Sr isotopic analyses for samples from different locations of the PMUB (Table 1). Representative mafic and ultramafic rock (basalts, gabbros, diorite and wehrlites) samples were collected in the Jagüé–Bonete, Rodeo, Sierra del Tigre, Sierra de la Invernada, Alto del Colorado, Calingasta Cerro Redondo, Peñasco, Pozos and Cortaderas areas (Figs 1, 2; Table 1). Each sample taken for analyses consisted of around 5 kg of unaltered material.

A total of 17 mafic–ultramafic rock samples from the Rodeo, Alto del Colorado, Sierra del Tigre and Sierra de la Invernada areas (Fig. 1) were analysed for whole-rock major-element oxides (SiO₂, TiO₂, Al₂O₃, FeO, MnO, MgO, CaO, Na₂O, K₂O and P₂O₅) and minor and trace elements (Li, Sc, V, Cr, Co, Ni, Cu, Zn, Ga, Rb, Sr, Y, Zr and Nb) (Table 2). The complete analytical procedure was performed in ALS Laboratory Group SL. It consisted of crushing, powder reduction and a lithium borate fusion of a minor fraction, prior to acid dissolution. Final dissolutions were analysed by X-ray fluorescence (XRF), major elements by inductively coupled plasma atomic emission spectroscopy (ICP-AES) and minor and trace elements by inductively coupled plasma mass spectrometry (ICP-MS).

In addition, mineral chemical analyses were performed on a total of 275 points (229 in clinopyroxene, 42 in plagioclase and 4 in ilmenite crystals) on 18 representative mafic samples (diorite, leuco-gabbro, microgabbros and gabbros) from the Sierra de la Invernada, Alto del Colorado, Sierra del Tigre, Calingasta and Peñasco areas (Figs 1, 2; online Supplementary Tables S1–S3, available at <http://journals.cambridge.org/geo>). The major-element composition of each mineral phase analysed was obtained using a JEOL JXA-8230 electron probe micro-analyser (EPMA) in the Laboratorio de Microscopía Electrónica y Análisis de Rayos X (LAMARX) of the Universidad Nacional de Córdoba (Argentina). Operating conditions involved a constant voltage intensity of 15 kV, a beam current of 20 nA and a beam diameter of 1–5 µm. For mineral phases, qualitative determinations were obtained using energy-dispersive spectrometers (EDS), and quantitative determinations were acquired by wavelength-dispersive spectrometers (WDS). In the last case, a combination of natural silicates and oxides were used for calibration: wollastonite (Si and Ca); anorthite (Si); anorthoclase (Na); orthoclase (Si, Al, K); sodalite (Cl); celestine (Sr); rutile (Ti); rhodonite (Mn); topaz (F), apatite (F, P and Ca); diopside

(Mg, Si and Ca); chromite (Mg, Cr and Al); ilmenite (Ti and Fe²⁺); hematite (Fe); vanadinite (V); nickeline (Ni); fayalite (Si and Fe²⁺); forsterite (Si and Mg); and hornblende (Mg, Al, Si, Ti and Ca). Other used standard oxides included MgO (Mg) and ZnO (Zn).

Whole-rock Nd and Sr isotopic analyses were performed on 28 mafic rock samples from the Jagüé–Bonete, Rodeo, Sierra del Tigre, Sierra de la Invernada, Calingasta, Cerro Redondo, Peñasco, Pozos and Cortaderas areas (Figs 1, 2; Table 3). From this dataset, 15 samples were analysed at the Laboratório de Geoquímica Isotópica e Geocronologia of the Universidade de Brasília (Brazil) following the method described by Gioia & Pimentel (2000). For the remaining 13 samples, ⁸⁷Sr/⁸⁶Sr and ¹⁴³Nd/¹⁴⁴Nd ratios were obtained in the Keck Isotope Laboratory at Cornell University (USA) by thermal ionization mass spectrometry (TIMS) on a VG Sector 54 system. All errors in measured samples and standards are 2σ. The constant decay of ¹⁴⁷Sm is $6.54 \times 10^{-12} \text{ a}^{-1}$ (Lugmair & Marti, 1978). ϵ_{Sr} and ϵ_{Nd} values were calculated using the chondritic uniform reservoir (CHUR) parameters of ⁸⁷Sr/⁸⁶Sr = 0.7045 and ¹⁴³Nd/¹⁴⁴Nd = 0.512638 (DePaolo & Wasserburg, 1976). $\epsilon_{Nd,i}$ and (⁸⁷Sr/⁸⁶Sr)_i contents were calculated at 418, 454 and 576 Ma. The criteria followed were based on two features: (1) maximum depositional ages and palynological and/or conodont-graptolite biostratigraphy; and (2) field observations and the proximity between the mafic intrusions studied in the Pozos and Cortaderas areas, and basalts with crystallization age of 418 Ma and 576 Ma (U–Pb on zircons) reported by Davis *et al.* (2000). In (1), the crystallization age of 454 Ma estimated by Fauqué & Villar (2003) is consistent with siliciclastic successions of Sandbian–Katian–Hirnantian fossil fauna hosted in the Yerba Loca, Sierra de la Invernada and Alcaparrosa formations from the northern PMUB (Furque, 1983; Ortega *et al.* 2008); and the crystallization age of 418 Ma assumed for samples from Cerro Redondo and Peñasco areas is based on flora findings reported by Cortés (1992) and estimated in basalts (U–Pb on zircons) by Davis *et al.* (2000).

When the crystallization age is unknown, the Nd model age represents the time at which the isotopic composition of the sample was identical to that of a certain model reservoir (CHUR or depleted mantle; DePaolo, 1988). In our study, depleted mantle Nd model ages were obtained using a single-stage model and ¹⁴³Nd/¹⁴⁴Nd = 0.51313 and ¹⁴⁷Sm/¹⁴⁴Nd = 0.24835 ratios (Workman & Hart, 2005). Nevertheless, care must be taken when using trace-element concentrations estimated by ICP-MS. The analytical uncertainty on this technique can lead to up to 10% error, and is propagated when determining the isotopic ¹⁴⁷Sm/¹⁴⁴Nd ratio (Lin *et al.* 2016). Calculated model ages can therefore be lower or higher than expected.

In order to better characterize the entire extension of the PMUB, we compiled a dataset of 80 published whole-rock geochemical analyses of mafic and ultramafic rocks from the northern and southern sectors of this belt. The combination of already published and new geochemical data presented in this work constitute a more robust database, representative of the 400-km-long PMUB, allowing us to correlate and compare different localities throughout it.

4. Results

4.a. Petrography

Mafic and ultramafic rocks studied in this contribution consist of N-trending sills, lenses, dykes or lava flows with widths dependent on the type of intrusion and its structure. These bodies are inter-layered with siliciclastic rocks (Fig. 3a) that show thin (< 5 cm)

Table 1. Summary table showing the dataset presented in this work, including analysed rock type, sample name, location, field relationship and study performed in each case

Area, sam- ple	Latitude (S), longitude (W)	Rock type	Field relationship	Whole-rock geochemistry	Mineral chemistry			Nd-Sr isotope analyses		P-T estima- tions
					Cpx	Pl	Ilm	¹⁴³ Nd/ ¹⁴⁴ Nd	⁸⁷ Sr/ ⁸⁶ Sr	
Northern PMUB										
Bonete										
3-18-2	28° 30', 68° 30'	Basalt	Lava flow					×	×	
Rodeo										
3-15-1	30° 12', 69° 04'	Basalt	Lava flow					×	×	
3-15-4	30° 12', 69° 04'	Microgabbro	Dyke					×	×	
R60	30° 11' 17.22", 69° 3' 2.92"	Basalt	Lava flow	×						
R70	30° 14' 59.98", 69° 3' 44.89"	Gabbro	Dyke	×						
PC4	30° 21' 53.54", 69° 4' 45.01"	Microgabbro	Sill	×						
Alto del Colordado										
COL1	30° 32' 45.87", 69° 6' 31.39"	Gabbro	Sill		×	×	×			×
COL8	30° 41' 52.93", 69° 0' 44.15"	Gabbro	Sill	×						
COL16B	30° 39' 2.80", 69° 6' 42.49"	Microgabbro	Sill	×						
Sierra del Tigre										
3-12-6	30° 52', 69° 19'	Basalt	Lava flow					×	×	
ST16	30° 45' 20.31", 69° 6' 22.99"	Microgabbro	Sill	×						
ST27B	30° 53' 57.25", 69° 8' 57.67"	Diorite	Sill	×			×			
ST55	30° 54' 22.67", 69° 10' 29.51"	Wehrlite	Sill	×				×	×	
ST61	30° 54' 29.80", 69° 10' 44.19"	Microgabbro	Dyke	×				×	×	
Sierra de la Invernada										
D1	30° 56' 59.59", 69° 4' 56.95"	Gabbro	Sill	×	×	×	×			×
G3	30° 57' 0.84", 69° 4' 56.93"	Gabbro	Sill	×	×	×		×	×	×
QDC2	30° 56' 58.15", 69° 4' 48.62"	Gabbro	Sill	×						
BAYO1	30° 57' 30.33", 69° 4' 18.78"	Leuco-gabbro- norite	Sill	×	×	×				×
QEA10	31° 0' 49.51", 69° 5' 18.21"	Gabbro	Sill	×	×	×		×	×	×
QLPD	30° 50' 1.07", 69° 3' 5.51"	Gabbro	Sill	×	×	×		×	×	
QLP5	30° 49' 50.90", 69° 3' 5.06"	Gabbro	Sill	×	×	×				×
QLP6	30° 49' 49.95", 69° 3' 1.18"	Gabbro	Sill	×	×	×	×			×
Calingasta										
3-12-2	31° 19' 46", 69° 24' 50"	Basalt	Lava flow					×	×	
G2	31° 21' 03", 69° 17' 17"	Gabbro	Sill		×					

(Continued)

Table 1. (Continued)

Area, sample	Latitude (S), longitude (W)	Rock type	Field relationship	Whole-rock geochemistry	Mineral chemistry			Nd–Sr isotope analyses		<i>P–T</i> estimations
					Cpx	Pl	Ilm	¹⁴³ Nd/ ¹⁴⁴ Nd	⁸⁷ Sr/ ⁸⁶ Sr	
KM025	31° 21' 03", 69° 17' 17"	Gabbro	Sill		×					
KM-ES01	31° 21' 03", 69° 17' 17"	Gabbro	Sill		×					
KM-ES3	31° 21' 03", 69° 17' 17"	Gabbro	Sill		×					
KM-ES4	31° 21' 03", 69° 17' 17"	Gabbro	Sill		×					
KM-ES5	31° 21' 03", 69° 17' 17"	Microgabbro	Lava flow		×					
KM-ES9*	31° 21' 03", 69° 17' 17"	Microgabbro	Dyke		×				×	
KM-ES10*	31° 21' 03", 69° 17' 17"	Microgabbro	Sill		×				×	
KM-ES11*	31° 21' 03", 69° 17' 17"	Microgabbro	Sill		×				×	
Southern PMUB										
Cerro Redondo										
CR 37-15	32° 14' 29.80", 69° 16' 2.00"	Microgabbro	Lava flow					×	×	
CR 38-15B	32° 15' 16.20", 69° 16' 6.70"	Basalt	Lava flow					×	×	
Peñasco										
QM 2-08	32° 11' 52.90", 69° 8' 15.60"	Microgabbro	Sill		×			×	×	
QM 2C-10	32° 11' 33.50", 69° 8' 30.20"	Microgabbro	Sill					×	×	
CPN 16-11	32° 12' 35.82", 69° 8' 40.80"	Microgabbro	Sill					×	×	
CPN 17-11	32° 12' 48.90", 69° 7' 36.20"	Microgabbro	Sill					×	×	
Pozos										
cga97-89	32° 16' 4.54", 69° 7' 22.87"	Microgabbro	Sill					×		
cga97-132a	32° 16' 42.06", 69° 8' 6.41"	Microgabbro	Sill					×		
QP 26-15	32° 16' 2.95", 69° 7' 24.68"	Gabbro	Sill					×		
Cortaderas										
usp94-18	32° 19' 12.83", 69° 8' 2.39"	Microgabbro	Sill					×		
usp97-1	32° 18' 51.30", 69° 8' 16.21"	Basalt	Lava flow					×		
usp94-51	32° 19' 57.99", 69° 8' 29.76"	Microgabbro	Sill					×		
QM 51A	32° 18' 56.80", 69° 8' 19.80"	Microgabbro	Sill					×	×	
QM 53	32° 19' 11.30", 69° 8' 6.30"	Gabbro	Sill					×	×	
usp97-8	32° 21' 16.54", 69° 9' 31.29"	Microgabbro	Dyke					×		
usp95-62	32° 20' 14.66", 69° 9' 33.23"	Microgabbro	Sill					×		
usp95-96	32° 21' 6.19", 69° 10' 22.81"	Microgabbro	Sill					×		

*Whole-rock major elements used for *P–T* estimations from Boedo *et al.* (2013)

Table 2. Whole-rock major-element (wt %) calculated anhydrous and trace-element (ppm) analyses of basalts, gabbros, diorite and wehrlite from the Rodeo, Alto del Colorado, Sierra del Tigre and Sierra de la Invernada areas (Figs 1, 2; Table 1)

Area	Rodeo			Alto del Colorado		Sierra del Tigre				Sierra de la Invernada							
Sample	R60 ^a	R70 ^b	PC4 ^b	COL8 ^c	COL16B ^c	ST16 ^c	ST27B ^d	ST55 ^d	ST61 ^c	D1 ^e	G3 ^f	QDC2 ^e	BAYO1 ^c	QEA10 ^e	QLPD ^c	QLP5 ^c	QLP6 ^c
Rock type	Basalt	Gabbro	Micro-gabbro	Gabbro	Micro-gabbro	Micro-gabbro	Diorite	Wehrlite	Micro-gabbro	Gabbro	Gabbro	Gabbro	Leuco-gabbro-norite	Gabbro	Gabbro	Gabbro	Gabbro
Major-element oxides (wt%)																	
SiO ₂	48.41	48.27	48.75	46.74	50.70	49.55	53.38	44.19	49.65	48.28	48.42	48.40	48.77	48.18	48.30	48.28	49.01
TiO ₂	2.38	1.63	2.50	1.41	2.00	2.19	2.01	0.83	2.29	2.18	1.98	2.09	1.92	1.62	1.60	3.01	2.01
Al ₂ O ₃	17.37	16.43	14.80	13.89	14.94	14.11	15.76	6.63	13.63	14.08	14.76	14.16	16.76	15.63	16.25	12.60	13.88
Fe ₂ O ₃	13.56	10.85	13.61	11.94	13.45	12.62	11.56	13.29	13.13	14.13	13.36	13.76	12.24	12.12	11.37	17.11	13.83
MnO	0.19	0.16	0.22	0.17	0.20	0.22	0.15	0.20	0.21	0.20	0.20	0.22	0.19	0.19	0.18	0.24	0.22
MgO	6.33	7.48	6.02	12.09	7.20	5.91	3.71	28.68	6.80	6.67	6.83	7.29	5.42	7.45	7.00	5.32	7.14
CaO	6.84	12.62	10.51	11.07	9.30	12.62	6.76	5.43	11.45	9.84	11.56	11.41	11.59	12.17	12.41	9.52	10.93
Na ₂ O	4.52	2.13	2.46	1.76	1.84	2.33	6.26	0.23	2.27	3.12	2.22	2.08	2.54	2.19	2.36	2.99	2.13
K ₂ O	0.07	0.20	0.77	0.53	0.05	0.17	0.13	0.11	0.26	1.18	0.40	0.38	0.34	0.21	0.34	0.65	0.58
Cr ₂ O ₃	0.03	0.07	0.02	0.12	0.03	0.03	–	0.31	0.04	0.02	0.03	0.02	0.01	0.05	0.02	–	0.03
P ₂ O ₅	0.24	0.10	0.25	0.20	0.17	0.22	0.22	0.08	0.21	0.22	0.19	0.15	0.19	0.15	0.11	0.22	0.18
SrO	0.02	0.04	0.05	0.05	0.05	0.04	0.05	0.02	0.03	0.07	0.04	0.03	0.03	0.03	0.04	0.05	0.04
BaO	0.03	0.01	0.04	0.01	0.06	0.01	0.01	–	0.02	0.02	0.01	0.01	–	–	0.01	0.01	0.02
Total	100.05	100.79	99.07	100.03	98.63	99.54	98.08	99.46	100.35	100.49	100.71	100.26	100.5	100.68	98.13	100.9	98.74
LOI	4.2	2.17	2.45	2.46	4.94	2.06	2.92	9.16	2.07	2.1	0.76	2.12	0.85	0.85	1.85	2.11	2.22
Mg no.	0.48	0.58	0.47	0.67	0.52	0.48	0.39	0.81	0.51	0.48	0.50	0.51	0.47	0.55	0.55	0.38	0.51
Trace elements (ppm)																	
V	320	283	380	248	358	401	95	137	404	353	355	354	326	313	298	620	381
Cr	190	470	160	890	200	190	10	1970	290	160	190	180	90	350	170	10	190
Co	42	48	39	59	44	38	35	97	44	49	50	51	41	45	44	55	48
Ni	75	148	69	351	92	78	8	1470	102	73	82	85	57	98	86	55	102
Cu	197	134	369	97	131	197	133	66	191	167	169	178	197	149	130	361	166
Zn	112	79	97	85	192	101	71	79	110	113	105	116	100	86	85	138	122
Ga	21.3	20.1	21.7	18.1	20.6	21.4	18.5	8.9	21.5	21.1	20.6	21.3	22.5	19.2	20.1	22.7	19.5
Rb	1.8	3.9	24.5	20.2	2.1	4.3	2.7	4.7	5.4	54.3	13	13.9	10.8	4.7	11.6	19.8	26.1
Sr	131	260	339	311	338	232	367	78.2	202	505	246	230	227	184.5	295	314	284
Y	26.5	21	28.5	20.9	22.2	29.6	28.5	9.1	28.3	26.9	24.7	26.3	28.3	24.5	19.7	29.1	24.1

(Continued)

Table 2. (Continued)

Area	Rodeo			Alto del Colorado			Sierra del Tigre				Sierra de la Invernada						
Sample	R60 ^a	R70 ^b	PC4 ^b	COL8 ^c	COL16B ^c	ST16 ^c	ST27B ^d	ST55 ^d	ST61 ^c	D1 ^e	G3 ^f	QDC2 ^e	BAYO1 ^c	QEA10 ^e	QLPD ^c	QLP5 ^c	QLP6 ^c
Rock type	Basalt	Gabbro	Micro-gabbro	Gabbro	Micro-gabbro	Micro-gabbro	Diorite	Wehrlite	Micro-gabbro	Gabbro	Gabbro	Gabbro	Leuco-gabbro-bronorite	Gabbro	Gabbro	Gabbro	Gabbro
Zr	138	99	157	102	113	133	146	46	143	125	107	118	123	100	82	144	114
Ba	283	65.9	416	81.2	539	98.3	78.3	41.8	155.5	164.5	131	114	59.9	43.5	82.9	101.5	219
Sc	34	36	35	34	39	42	18	17	40	41	41	39	36	41	39	43	37
Nb	11.3	7.6	13.6	7.6	10	10.3	9.6	3.5	11	10	9.3	9.7	8.8	7.1	7	12.2	14.8
Cs	0.3	0.18	1.04	0.91	0.3	0.28	0.32	2.7	0.34	0.72	0.55	0.55	0.81	0.68	0.8	0.85	0.58
U	0.39	0.19	0.39	0.28	0.3	0.25	0.4	0.14	0.27	0.27	0.2	0.23	0.22	0.19	0.16	0.25	0.26
Th	0.87	0.59	1.04	0.69	0.77	1.71	1.53	0.4	0.85	0.8	0.65	0.73	0.7	0.51	0.48	0.81	0.82
Hf	3.8	2.9	4.1	2.8	3.1	3.4	3.6	1.3	3.8	3.6	3	3.3	3.2	2.9	2.4	3.7	3
Ta	0.7	0.5	0.8	0.5	0.7	0.6	0.6	0.3	0.7	0.6	0.6	0.6	0.6	0.4	0.4	0.8	1
La	10.4	7.4	12.1	8.2	9	9.5	10.2	3.4	10.6	9.8	8.5	9.5	8.4	6.8	6.6	10.8	8.4
Ce	25.3	17.5	29.9	18.9	22.4	24.2	25.7	8.3	26.9	23.5	20.6	22.8	20.3	16.6	15.7	26.7	21.6
Pr	3.7	2.61	4.3	2.65	3.25	3.51	3.83	1.25	3.93	3.28	2.89	3.32	2.89	2.51	2.32	3.97	3.12
Nd	18	12.1	20.4	13.8	15.7	17.4	17.6	6.2	18.9	16.3	14.5	16	14.9	11.8	11.7	18.4	15.2
Sm	4.63	3.56	5.67	3.37	4.2	4.67	4.9	1.57	5.47	4.86	4.42	4.16	4.22	3.59	3.59	5.32	4.47
Eu	1.52	1.19	1.9	1.22	1.44	1.58	1.64	0.57	1.7	1.59	1.51	1.66	1.49	1.35	1.37	1.89	1.47
Gd	5.61	4.24	6.23	4.25	4.97	5.85	5.55	1.81	6.3	5.62	5.08	5.53	5.48	4.76	4.08	6.18	4.99
Tb	0.84	0.64	1	0.7	0.74	0.93	0.88	0.28	0.96	0.93	0.78	0.85	0.87	0.79	0.6	0.94	0.8
Dy	5.22	4.13	6.32	3.98	4.71	5.85	5.6	1.79	5.82	5.31	4.73	5.24	5.49	4.89	3.89	6.06	4.96
Ho	1	0.85	1.16	0.83	0.9	1.18	1.09	0.37	1.1	1.07	0.93	1.02	1.12	0.99	0.77	1.22	0.96
Er	3.01	2.08	3.34	2.36	2.57	3.5	2.93	0.91	3.1	3.01	2.59	2.96	3.14	2.91	2.08	3.24	2.56
Tm	0.39	0.32	0.45	0.31	0.29	0.43	0.41	0.11	0.42	0.43	0.37	0.38	0.44	0.39	0.29	0.47	0.36
Yb	2.5	1.87	2.7	1.86	1.9	2.88	2.8	0.94	2.75	2.49	2.44	2.35	2.97	2.58	1.98	2.85	2.44
Lu	0.38	0.27	0.43	0.28	0.29	0.43	0.42	0.13	0.41	0.33	0.3	0.34	0.37	0.33	0.26	0.44	0.33

Primary texture: ^aporphyritic-intersertal; ^bhipidiomorphic inequigranular subophitic; ^chipidiomorphic inequigranular ophitic; ^dhipidiomorphic equigranular; ^ehipidiomorphic equigranular ophitic-subophitic; ^fhipidiomorphic inequigranular poikilitic.

Table 3. Nd and Sr isotope data of mafic rocks from different localities of the PMUB (Figs 1, 2; Table 1). $\epsilon_{Nd}(t)$ values are calculated using crystallization ages obtained in basalts (U–Pb on zircon) from the Jagüé-Bonete and Cortaderas areas (Davis *et al.* 2000; Fauqué & Villar, 2003)

Locality	Sample	Rb (ppm)	Sr (ppm)	$^{87}\text{Rb}/^{86}\text{Sr}$	$^{87}\text{Sr}/^{86}\text{Sr}$	$(^{87}\text{Sr}/^{86}\text{Sr})_i$	Sm (ppm)	Nd (ppm)	$^{147}\text{Sm}/^{144}\text{Nd}$	$^{143}\text{Nd}/^{144}\text{Nd}$	ϵ_{Nd}	$(^{143}\text{Nd}/^{144}\text{Nd})_i$	$\epsilon_{Nd,i}$	T_{DM} (Ma)	Age (Ma)
Bonete	3-18-2	–	276	–	0.7044477	–	4.35	14.90	0.1758	0.5129147	5.4	0.512392	6.6	456.93	454
Rodeo	3-15-1	–	286	–	0.703426	–	5.16	19.13	0.1624	0.5128973	5.1	0.512414	7.0	416.26	454
	3-15-4	–	–	–	0.7040124	–	6.63	24.70	0.1616	0.5129228	5.6	0.512442	7.6	367.29	454
Sierra del Tigre	3-12-6	–	315	–	0.7033754	–	4.71	15.70	0.1806	0.5129243	5.6	0.512387	6.5	468.22	454
	ST27B	2.7	367	0.020	0.707430	0.70730	3.89	14.32	0.1640	0.512767	2.5	0.512279	4.4	656.94	454
	ST55	4.7	78.2	0.165	0.704610	0.70354	2.83	6.57	0.2610	0.513260	12.1	0.512484	8.4	1592.33	454
	ST61	5.4	202	0.074	0.703490	0.70301	4.37	15.77	0.1680	0.512890	4.9	0.512390	6.6	452.91	454
Sierra de la Invernada	G3	13	246	0.145	0.711740	0.71080	4.56	16.58	0.1660	0.512898	5.1	0.512404	6.8	430.64	454
	QLPD	4.7	184.5	0.070	0.705170	0.70472	3.38	12.54	0.1630	0.512907	5.2	0.512422	7.2	397.37	454
	QEA10	11.6	295	0.108	0.705580	0.70488	3.59	12.42	0.1750	0.512868	4.5	0.512348	5.7	543.71	454
Calingasta	3-12-2	–	218	–	0.705331	–	3.78	11.90	0.1913	0.512966	6.4	0.512397	6.7	444.17	454
Cerro Redondo	CR 37-15	–	–	–	0.708330	–	3.71	12.57	0.1780	0.512953	6.1	0.512466	7.1	386.35	418
	CR 38-15B	–	–	–	0.710890	–	5.83	23.51	0.1500	0.512857	4.3	0.512446	6.8	423.01	418
Peñasco	QM 2-08	24	477	0.139	0.708720	0.70790	2.93	10.23	0.1730	0.512915	5.4	0.512441	6.7	436.69	418
	QM 2C-10	2	769	0.007	0.714390	0.71435	3.12	10.06	0.1870	0.512885	4.8	0.512373	5.3	611.41	418
	CPN 16-11	5	695	0.020	0.708330	0.70821	4.79	17.17	0.1690	0.512909	5.3	0.512446	6.8	423.42	418
	CPN 17-11	4	253	0.044	0.706730	0.70647	3.15	10.73	0.1780	0.512915	5.4	0.512428	6.4	463.39	418
Pozos	cga97-89 ^a	–	317	–	–	–	5.12	18.00	0.1713	0.512890	4.9	0.512421	6.3	479.01	418
	cga97-132a	–	647	–	–	–	4.24	15.83	0.1613	0.512897	5.1	0.512897	6.9	411.43	418
	QP 26-15	–	–	–	–	–	6.12	16.88	0.2190	0.512875	4.6	0.512275	3.4	1327.34	418
Cortaderas	usp94-18	–	226	–	–	–	3.56	11.50	0.1864	0.512906	5.2	0.512203	6.0	556.80	576
	usp97-1	–	196	–	–	–	4.92	16.96	0.1748	0.512862	4.4	0.512203	6.0	559.92	576
	usp94-51 ^a	–	321	–	–	–	3.77	12.55	0.1810	0.512916	5.4	0.512233	6.6	490.12	576
	QM 51A	6	255	0.065	0.707300	0.70677	4.89	16.96	0.1740	0.512824	3.6	0.512167	5.3	628.78	576
	QM 53	5	271	0.051	0.705560	0.70514	4.42	13.68	0.1950	0.512869	4.5	0.512133	4.6	750.13	576
	usp97-8	–	380	–	–	–	6.90	26.25	0.1564	0.512864	4.4	0.512436	6.6	453.68	418
	usp95-62	–	764	–	–	–	2.30	9.30	0.1491	0.512868	4.5	0.512460	7.0	405.71	418
	usp95-96	–	666	–	–	–	5.00	20.20	0.1490	0.512881	4.7	0.512473	7.3	385.41	418

^aCrystallization ages of 576 ± 17 Ma and 418 ± 10 Ma (U–Pb on zircon) obtained by Davis *et al.* (2000)

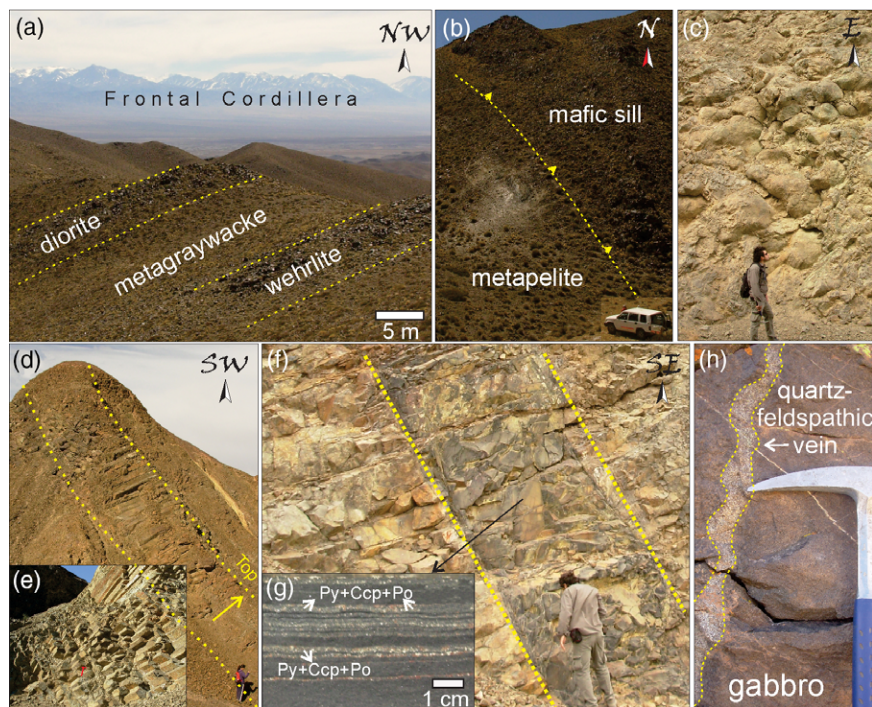


Fig. 3. (Colour online) Field relationship between igneous and metasedimentary rocks. (a) Yerba Loca Formation at the Sierra del Tigre area. Diorite and wehrlite sills interlayered with metagraywacke. (b) Yerba Loca Formation at the Sierra del Tigre area. Thick gabbro sill in tectonic contact with metapelitic layers. (c) Yerba Loca Formation at the Rodeo area. Basaltic lava flows (view from the top-side) with pillow-shaped structure. (d) Yerba Loca Formation at the Rodeo area. Thick basaltic flow with columnar jointing. (e) Detail of the columnar-shaped jointing shown in (d). (f) Yerba Loca Formation at the Rodeo area. Sulphide-bearing metapelite layers. (g) Detailed view of sulphide-bearing metapelite. Sulphide layers consist of euhedral $\text{Py} \pm \text{Ccp} \pm \text{Po}$ (mineral abbreviations after Whitney & Evans, 2010). (h) Sierra de la Invernada Formation at the homonymous area. Gabbro sill dissected by quartz-feldspathic vein. The yellow dashed lines in (a, b, d, f) separate mafic from metasedimentary units. The yellow dotted line in (h) separates a quartz-feldspathic vein corresponding to a gabbroic sill. See location areas in Figures 1 and 2.

dark chilled margins, or are in tectonic contact with greenish shale and metapelites (Fig. 3b) from the Yerba Loca, Alcaparrosa and Sierra de la Invernada formations.

Mafic dykes and basaltic lava flows are the major bodies in the Rodeo, Alto del Colorado and Calingasta areas (Fig. 2). They exhibit columnar jointing and a pillow-shaped structure (Fig. 3c–e) with thicknesses ranging over 3–20 m. Volcanic textures are microgranular to porphyritic with a microcrystalline or partly glassy matrix containing a few phenocrysts of plagioclase and clinopyroxene. These mafic flows are interbedded with sulphide-bearing metapelites, with parageneses consisting of disseminated or thin massive layers (< 4 mm) of euhedral $\text{Py} \pm \text{Ccp} \pm \text{Po}$ (mineral abbreviations after Whitney & Evans, 2010) (Fig. 3f, g). Similar sulphide concentrations comprising Py, Ccp, Gn, Sp, Ttr, Mrc, Apy, Au and Mol have been found in the Calingasta area by Brodtkorb *et al.* (2015). In basaltic lava flows from the Rodeo and Calingasta areas, spaces between the individual pillows and their vesicles are filled with chert and calcium carbonate.

Mafic and ultramafic sills and lenses are the dominant intrusions in the Sierra del Tigre and Sierra de la Invernada areas (Fig. 2). They consist of massive layers with granular texture, of thicknesses 10–150 m, and exhibit onion-skinned weathering depending on grain size, which varies over 2–10 mm. Mafic sills studied in the Sierra de la Invernada area consist of dark-green fine- to coarse-grained gabbros with cross-cutting veins of quartz-feldspathic composition (Fig. 3h). It is worth noting that thicker bodies display magmatic layering of thickness from a few centimetres up to 2 m, alternating pyroxene- and plagioclase-rich bands, with variably modal crystal

concentrations. The Sierra del Tigre mafic rocks (Fig. 2) exhibit a wider textural and compositional range. Basaltic lava flows exposed at the western flank of the range exhibit massive and pillow structure, whereas the eastern flank of the range is dominated by massive diorite (Fig. 4a, b), dark-green fine-grained gabbros, coarse-grained gabbros (Fig. 4c, d) and wehrlite lenses (Fig. 4e, f) interbedded with metasandstone and metagreywacke.

Thin-section analyses in mafic and ultramafic rocks from the Sierra de la Invernada and Sierra del Tigre areas show a primary mineral association characterized by idiomorphic to hypidiomorphic 2–10-mm-long crystals with fine- to medium-grained (Fig. 4b), ophitic to subophitic (Fig. 4d) and, in some cases, poikilitic texture. Gabbros exhibit augite oikocrysts enclosing smaller crystals of Ca-rich plagioclase (Fig. 4d). Poikilitic texture suggests that plagioclase grew simultaneously or slightly earlier than clinopyroxene. Recognized skeletal texture supports the simultaneous growing of both minerals. Primary modal composition in these mafic rocks consists of clinopyroxene (Aug) varying over 4–48%, Ca-rich plagioclase (An_{66-86}) of up to 58%, accessory minerals ($\text{Mag} \pm \text{Ttn} \pm \text{Ilm}$) of up to 13%, quartz of up to 10%, olivine of up to 17%, hornblende of up to 6% and biotite of up to 5%.

Two partially serpentinized wehrlite sills exposed in Rodeo and Sierra del Tigre (Figs 1, 2) consist of euhedral to subhedral olivine relics (in a modal concentration of c. 70%), replaced by serpentine-group minerals and clinopyroxene (sample ST55 in Fig. 4f).

Mafic intrusions show partial pervasive alteration of the primary mineral assemblage mentioned above. Plagioclase is variably saussuritized to epidote, albite, calcite, white mica (sericite) and

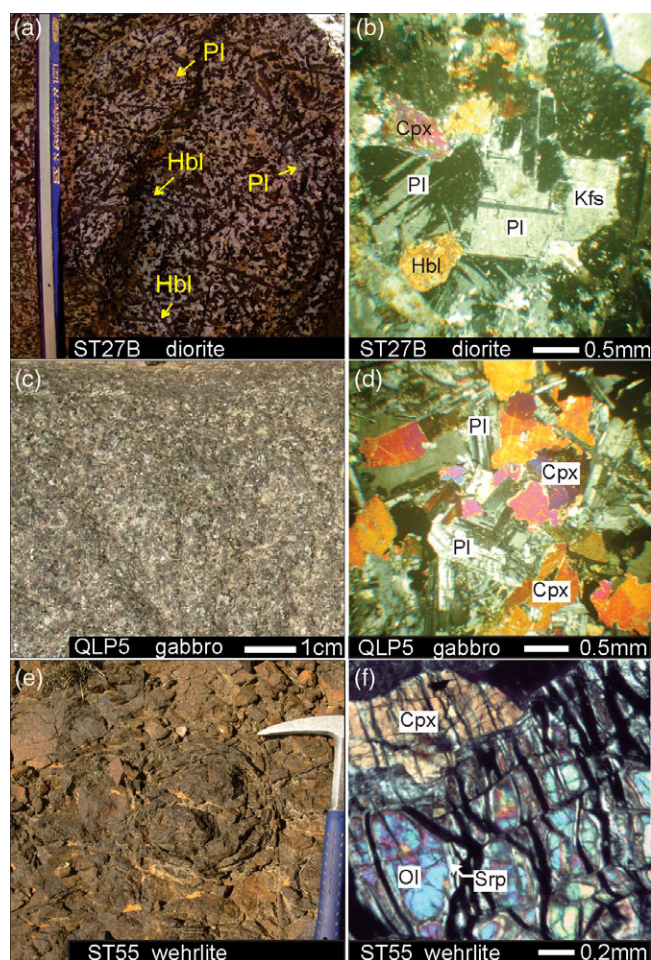


Fig. 4. (Colour online) (a) Fine- to medium-grained diorite hand specimen showing dark-green acicular hornblende and tabular plagioclase crystals. (b) Cross-polarized light photomicrograph showing the diorite of (a). Subidiomorphic fine-grained texture consists of partially altered plagioclase, potassium feldspar, clinopyroxene and hornblende crystals. (c) Greenish coarse-grained gabbro hand specimen. (d) Cross-polarized light photomicrograph of the gabbro shown in (c), which shows subidiomorphic ophitic-subophitic texture. (e) Coarse-grained wehrlite outcrop showing onion-skinned weathering. (f) Cross-polarized light photomicrograph of the wehrlite shown in (e) exhibiting coarse-grained texture with partially serpentinized olivine and clinopyroxene crystals. Mineral abbreviations after Whitney & Evans (2010).

clay minerals. Clinopyroxene is mainly fresh but sometimes presents embayed texture due to the replacement of minerals with a groundmass of secondary mineral assemblage. Many gabbros exhibit uraltized (Act + Chl) clinopyroxene rims. Olivine is mostly present as relict crystals with an almost complete alteration to serpentine-group minerals.

All recognized textures are magmatic with no sub-solidus deformation patterns identified. The secondary mineral assemblage mentioned above indicates a prehnite-pumpellyite to greenschist facies metamorphism and is consistent with previous observations in the Rodeo, Calingasta and Sierra del Tigre areas (Rubinstein *et al.* 1997; Robinson *et al.* 2005; González-Menéndez *et al.* 2013).

4.b. Mineral chemistry

4.b.1. Clinopyroxene

Clinopyroxene composition yields Ti_2O and Al_2O_3 contents in the ranges 0.12–1.74 wt% and 0.4–4.5 wt%, respectively. Magnesium

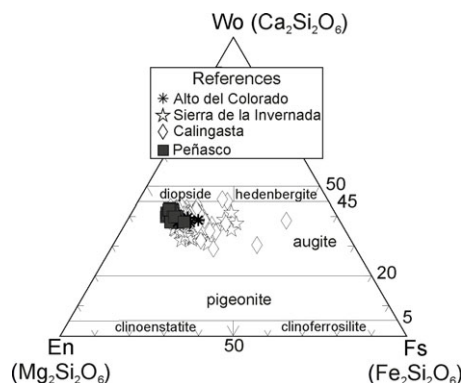


Fig. 5. Pyroxene classification diagram (Morimoto, 1988). Most analysed clinopyroxene crystals are augite, whereas only one measurement corresponds to a diopside composition with $Wo > 45$ (sample KMES3 from Calingasta area).

no. ($= 100 \times Mg / (Mg + Fe)$) is 16–74 and correlates positively with the Al_2O_3 content. Wollastonite (Wo), Enstatite (En) and Ferrosillite (Fs) contents are 29–45.5, 15.3–49.7 and 10–46.2, respectively (online supplementary Table S1). An evolution towards the Fs end-member in gabbro crystals can be recognized (Fig. 5). Analysed clinopyroxene crystals are augite, whereas only one measurement corresponds to a diopside composition with $Wo > 45$ (sample KMES3 from Calingasta area).

Most of the analysed clinopyroxenes are chemically homogeneous. Nevertheless, a few crystals exhibit a continuous magmatic zoning with a decrease in Al_2O_3 and CaO contents and an increase in FeO, Na_2O and Ti_2O contents from core to rims (sample QM208px02 in Fig. 6a–d). This zoning pattern is expected in crystals that follow the crystallization sequence of Ol + Pl + Cpx in basaltic magmas (Beccaluva *et al.* 1989). However, most of the zoned crystals exhibit a heterogeneous zoning with FeO, CaO and MgO contents varying throughout fractures and cleavage planes, suggesting post-magmatic hydrothermal alteration (sample QEA10px01, shown in Fig. 6e–h).

The majority of analysed points plot in the subalkaline ocean-floor basalts field and show a tholeiitic affinity (Fig. 7a, b). Some crystals from the Calingasta and Sierra de la Invernada locations lie in the alkaline field. Most of the analysed crystals exhibit an N-MORB to transitional and E-MORB affinity, suggested by a shift towards the TiO_2 – Na_2O boundary (Fig. 7c).

4.b.2. Plagioclase

Analysed crystals from samples collected in the northern region provide evidence of two groups of different composition (online Supplementary Table S2). One group is represented by heterogeneous normally zoned crystals with cores richer in anorthite than rims. These crystals present thin albitized rims and their nuclei are mostly altered to saussurite. Anorthite content is in the range of 34–85.6 from rim to core (e.g. Pl2 in sample G3, and Pl5 in sample BAYO1). In contrast, the other group comprises chemically homogeneous plagioclases, with anorthite content varying over 60.4–66.1 from rim to core (e.g. Pl1 in sample G3 and Pl4 in sample BAYO1).

4.b.3. Accessory minerals

Accessory minerals comprise ilmenite and titanite coexisting with hematite and magnetite. Ilmenite and titanite occur mostly as exsolved phases in clinopyroxene crystals or as individual

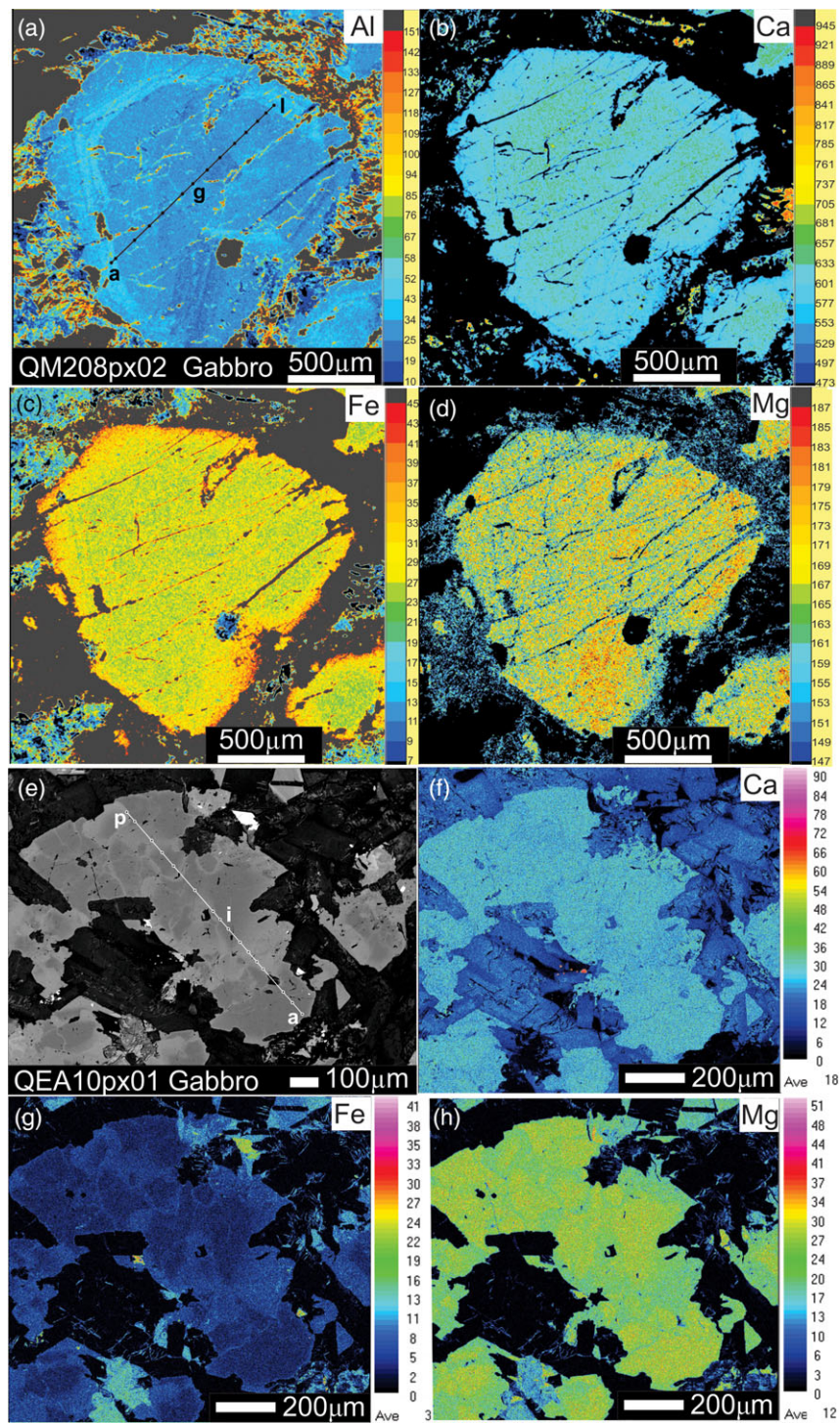


Fig. 6. (Colour online) Electron microprobe major-element mapping on pyroxene crystals of (a–d) sample QM208px02 from the Peñasco area and (e–h) sample QEA10 from the Sierra de la Invernada area. (a) Al distribution map. The black line indicates spot analysis along transverse a(rim) – g(core) – l(rim), as detailed in online supplementary Table S1. (b) Ca distribution map. (c) Fe distribution map. (d) Mg distribution map. The crystal (a–d) shows homogeneous magmatic zoning. (e) Backscattered electron image of pyroxene ‘px1’ of sample QEA10. The white line indicates spot analyses along transverse: a(rim) – i(core) – p(rim), as detailed in online supplementary Table S1. (f) Ca distribution map. (g) Fe distribution map. (h) Mg distribution map. Notice the heterogeneous zoning observed throughout fractures and cleavage surfaces (e–h).

subhedral grains in the matrix. A micro-intergrowth between ilmenite and titanite is recognized as ilmenite lamellae along the {111} planes of the titanite host, resulting in a Trellis texture. Ti_2O content of ilmenite is in the range of 47–51 wt%, whereas FeO ranges over 45–47 wt% and MnO over 1.9–2.9 wt%. Al_2O_3 ,

MgO and CaO contents are lower than 0.3 wt% (online Supplementary Table S3).

Other minor accessory phases observed in gabbros and diorite comprise euhedral to subhedral magnetite, zircon, baddeleyite and ulvöspinel.

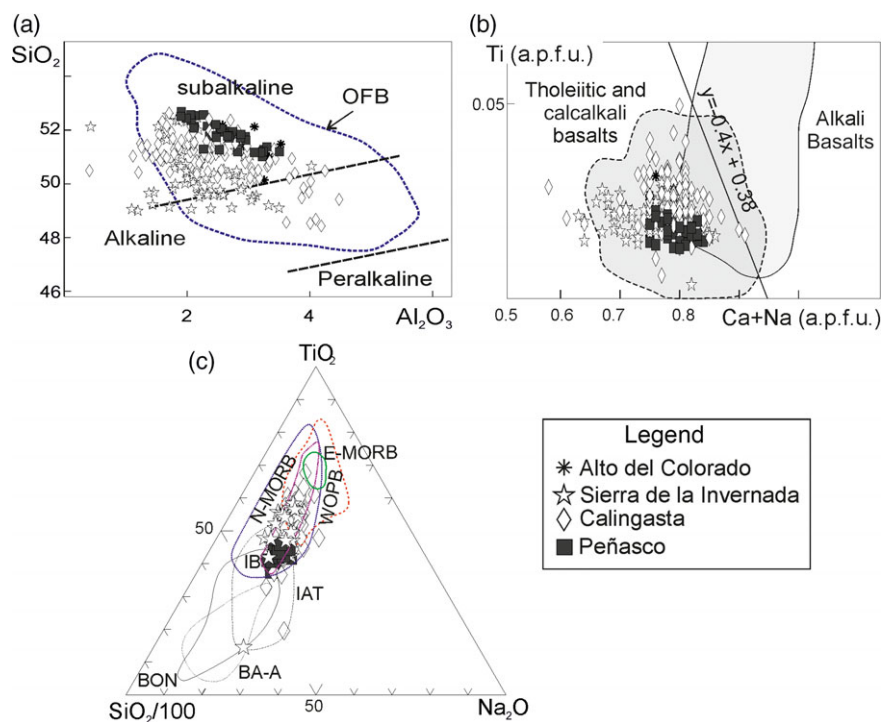


Fig. 7. (a) SiO_2 versus Al_2O_3 pyroxene diagram. Fields in dashed black lines are from Le Bas (1962). Analysed samples lie in the subalkaline ocean floor basalts field. (b) Ti versus $\text{Ca} + \text{Na}$ discrimination diagram (Leterrier *et al.* 1982). Most of the data plot in the tholeiitic and calcalkali basalts field. (c) $(\text{TiO}_2 - \text{Na}_2\text{O} - \text{SiO}_2)/100$ discrimination diagram (Beccaluva *et al.* 1989). The majority of the analysed crystals lie between the N-MORB to transitional and E-MORB fields. E-MORB – enriched mid-ocean-ridge basalt; N-MORB – normal mid-ocean-ridge basalt; WOPB – within-oceanic-plate basalt; IB – Iceland basalt; IAT – island-arc tholeiite; BON – boninite; BA-A – basaltic andesite and andesite.

4.c. Whole-rock geochemistry

4.c.1. Major elements

The studied mafic–ultramafic rocks from the Rodeo, Alto del Colorado, Sierra del Tigre and Sierra de la Invernada localities display highly variable loss on ignition (LOI) values (1.2–9.2 wt%), indicative of low-grade metamorphism and/or hydrothermal alteration. The highest value displayed in the wehrlite sample ST55 can be attributed to serpentinization (Fig. 4f). Major oxides present in a wide compositional range are SiO_2 (44.2–53.4 wt%), Al_2O_3 (6.6–17.4 wt%), MgO (3.7–28.7 wt%) and CaO (5.4–12.6 wt%) (Table 2). $\text{Fe}_2\text{O}_{3(\text{tot})}$ concentration is high (10.8–17.1 wt%), whereas TiO_2 is relatively high (0.8–3 wt%) and K_2O content is variable (0.1–1.2 wt%).

Major-element data presented on Harker-type bivariate plots (Fig. 8) exhibit partially scattered patterns, but some trends such as increasing SiO_2 , $\text{Na}_2\text{O} + \text{K}_2\text{O}$, Ti_2O and P_2O_5 for decreasing Mg no. ($100 \times \text{MgO}/(\text{MgO} + \text{FeO})$ calculated on a molar basis), can be recognized. CaO , $\text{Fe}_2\text{O}_{3(\text{tot})}$ and MnO concentrations display the most scattered distribution with increasing Mg no. (Fig. 8). The distribution trend in some major oxides (TiO_2 , Fe_2O_3 , CaO) can be attributed to variable fractionation and/or crystallization of minerals such as pyroxene, ilmenite, magnetite and titanite.

4.c.2. Trace elements

Ni content varies over 8–1470 ppm (with the highest value in wehrlite ST55) and has a good increasing correlation with Mg no. (Fig. 8), according to the degree of differentiation. In particular, samples with modal olivine show a positive correlation of Mg

no. with compatible elements (Cr and Ni). This trend indicates fractionation and/or accumulation of olivine.

Low-grade metamorphism and/or hydrothermal alteration may lead to selective element mobility. The highest value displayed in the wehrlite sample ST55 can be attributed to serpentinization (Fig. 4f). We therefore consider mainly high-field-strength elements (HFSEs) and REEs for petrogenetic interpretation and diagram discrimination since they are relatively immobile under conditions of alteration processes (e.g. Pearce, 2008).

All the studied mafic rocks are subalkaline basalts according to the Zr/Ti versus Nb/Y diagram (Winchester & Floyd, 1977; Fig. 9a). The studied samples show a well-defined transitional affinity (Fig. 9b), in agreement with previous studies performed in other sectors of the PMUB (e.g. Kay *et al.* 1984; Boedo *et al.* 2013; González-Menéndez *et al.* 2013). In the V-Ti discrimination diagram (Shervais, 1982), the majority of the samples plot in the CFB and MORB/back-arc basalt (BAB) fields (Fig. 9c). The variable V/Ti ratios of samples ST55, ST27B and QLP5 could have been controlled by magnetite fractionation throughout their evolution (Woodhead *et al.* 1993).

The trace-element composition of the analysed mafic–ultramafic rocks is characterized by: (1) a moderate LILE/HFSE ratio; and (2) LREE-enriched patterns with La/Sm ratios in the range 1.8–2.4 and Sm/Yb of 1.4–2.2 (Fig. 10a, b). The primordial mantle-normalized spider diagram indicates a scattered LILE distribution indicated by positive Cs anomaly, positive Ba anomaly, and low Rb, K and Sr content. Nevertheless, the gabbroic sample D1 exhibits higher Rb, K and Sr content. Moderately negative Th and P anomalies are also observed (Fig. 10a). Note that, with the exception of the wehrlite sample ST55, no negative Nb–Ta anomalies are observed.

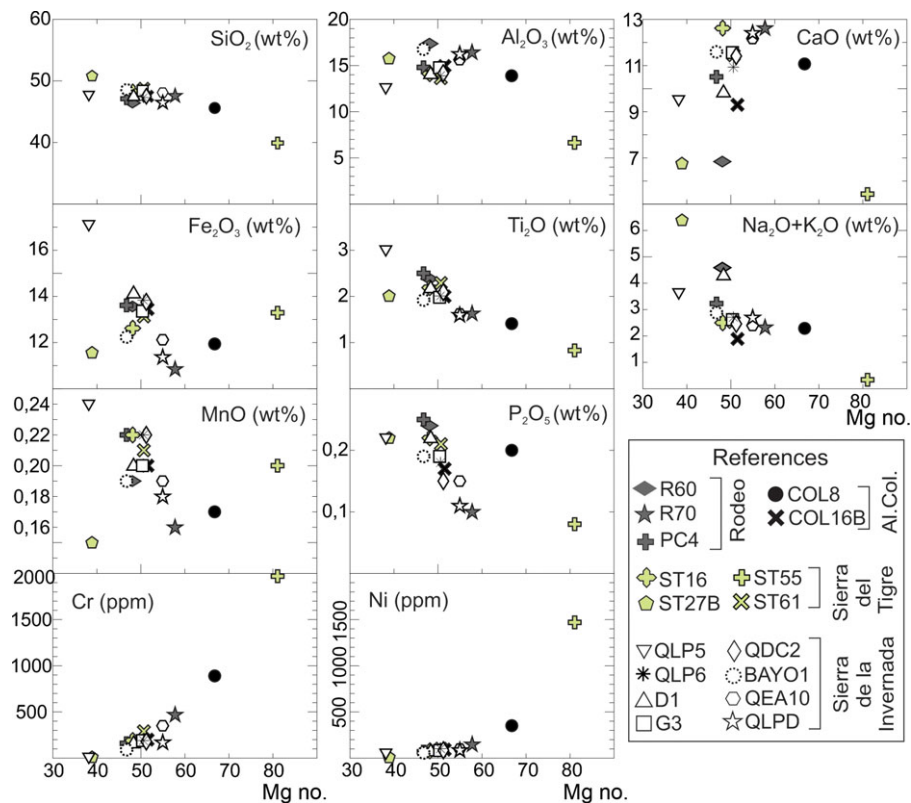


Fig. 8. (Colour online) Whole-rock major-element variations (wt%) versus Mg no. ($=100 \times \text{wt}\% \text{MgO} / (\text{MgO} + \text{FeO})$) calculated on a molar basis for mafic and ultramafic samples from the Rodeo, Alto del Colorado (Al. Col.), Sierra del Tigre and Sierra de la Invernada areas (see details in Table 2 and locations in Figs 1 and 2). Note the negative correlations of SiO_2 , $\text{Na}_2\text{O} + \text{K}_2\text{O}$, Ti_2O , and P_2O_5 , and the positive correlation of Cr and Ni versus Mg no.

Chondrite-normalized REE patterns are 10–70 times higher than chondrite values (except for the wehrlite sample ST55) (Fig. 10b). The moderate LREE/HREE ratio with $(\text{La}/\text{Yb})_N$ ranging over 1.9–3.4 indicates that garnet was not crystallized and was not an important residual source mineral in a shallow depth magma chamber (Green & Ringwood, 1967). Slightly positive Eu anomalies ($\text{Eu}/\text{Eu}^* = 0.88\text{--}1.09$, where $\text{Eu}^* = \sqrt{(\text{Sm}_N \times \text{Gd}_N)}$) indicate scarce or no plagioclase fractionation.

4.d. Nd and Sr isotope composition

The $\epsilon_{\text{Nd}(418)}$ values range between +3.4 and +7.2, $\epsilon_{\text{Nd}(454)}$ between +4.4 and +8.4, and $\epsilon_{\text{Nd}(576)}$ between +4.6 and +6.5 (Table 3). Overall, Nd isotope compositions are lower than those expected for MORB isotopic signatures with ϵ_{Nd} c. 10 (DePaolo, 1988). $^{87}\text{Sr}/^{86}\text{Sr}$ ratios have values ranging over 0.7030–0.7143, with the lowest value in gabbro ST61 and the highest value in basalt QM 2C-10 (Table 3). The large dispersion observed at relative constant ϵ_{Nd} values can be explained by Rb addition and Sr loss, likely due to post-emplacement alteration or hydrothermal alteration by means of seawater addition (McCulloch *et al.* 1980). The sample suite defines an array starting at the mantle array with a shift to a more radiogenic $(^{87}\text{Sr}/^{86}\text{Sr})_i$ ratio as $\epsilon_{\text{Nd},i}$ slightly decreases (except for sample QEA10) (Fig. 11). In particular, a group of samples from the Sierra del Tigre, Sierra de la Invernada and Cortaderas areas lie in the ocean island basalts (OIB) field between the depleted mantle (DM) and bulk silicate earth (BSE) end-members, and overlap the HIMU (high μ ; $\mu = ^{238}\text{U}/^{204}\text{Pb}$) and PREMA (PREvalent MAnTle) mantle reservoirs fields (Zindler & Hart,

1986). Nd isotope compositions in the range of overall analysed samples are comparable with those estimated for primitive continental flood basalts (Fig. 11). Despite the large range in $(^{87}\text{Sr}/^{86}\text{Sr})_i$ ratios, the uniform $\epsilon_{\text{Nd},i}$ for the analysed samples indicates a derivation from a common mantle source and clearly demonstrate an oceanic affinity. However, the Nd and Sr isotopic data cannot by themselves be used to precisely discriminate among different tectonic settings.

Nd T_{DM} ages estimated in the studied mafic rocks of the PMUB range over 1592–367 Ma (Table 3). From the overall analysed samples, only two (ST55 from the northern and QP26–15 from the southern sector), exhibit Mesoproterozoic T_{DM} ages of 1592 and 1327 Ma, respectively. A minor group of samples shows Neoproterozoic ages (750–611 Ma), whereas another group lies within the Precambrian–Cambrian boundary (560–544 Ma). The majority of the estimated T_{DM} ages are in the range of 490–367 Ma, representing the late Cambrian – Late Devonian interval.

5. Integration of obtained results and previous studies of the PMUB

5.a. Trace-element analysis and tectonic discrimination

Whole-rock geochemical analyses presented in this contribution are interpreted in the framework of available already published geochemical data at different locations of the PMUB: Jagüé-Bonete (Kay *et al.* 1984; Fauqué & Villar, 2003), Rodeo (Kay *et al.* 1984), Sierra del Tigre (Kay *et al.* 1984; González-Menéndez *et al.* 2013), Calingasta (Kay *et al.* 1984; Boedo *et al.*

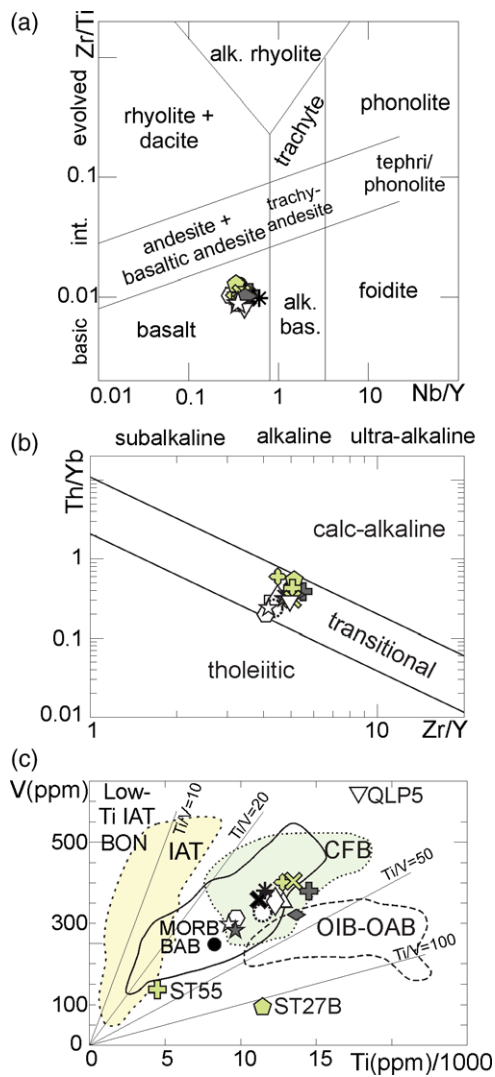


Fig. 9. (Colour online) (a) Zr/Ti versus Nb/Y discrimination diagram (Winchester & Floyd, 1977). Studied samples lie in the basic-subalkaline-basaltic field. (b) Th/Yb versus Zr/Y discrimination diagram (Ross & Bédard, 2009). Studied mafic rocks show a clear transitional signature. Some of them lie close to the tholeiitic field. (c) V–Ti diagram (after Shervais, 1982). Analysed samples (except ST55, ST27B and QLP5) plot in the continental flood basalts (CFB) and mid-ocean-ridge/back-arc-basin basalts (MORB-BAB) fields. BON – boninite; IAT – island-arc tholeiitic basalts; OIB – oceanic-island basalts; OAB – oceanic-alkaline basalts. Legend as in Figure 8.

2013), Peñasco (Boedo *et al.* 2013), Cerro Redondo (Cortés & Kay, 1994; Cortés *et al.* 1999), and Cortaderas and Bonilla (Boedo *et al.* 2013; Gregori *et al.* 2013). Combining all of the geochemical data from different localities within the PMUB in a single dataset allows us to understand the magmatic and tectonic setting related to the origin of the mafic rocks.

Mafic rocks from the northern sector of the PMUB (Fig. 12a) are characterized by a low to moderate LREE slope with a (La/Sm)_N ratio ranging over 1.1–2.5, and a low to moderate HREE slope with a (Sm/Yb)_N ratio ranging over 1.1–3.2. The LREE fractionation trends in samples from the Rodeo and Sierra del Tigre areas are broadly parallel to that of CFBs, with a few samples more or less enriched in LREE elements. In addition, they are more fractionated in comparison with the E-MORB trend, except for HREE in most of the samples. Ultramafic rocks

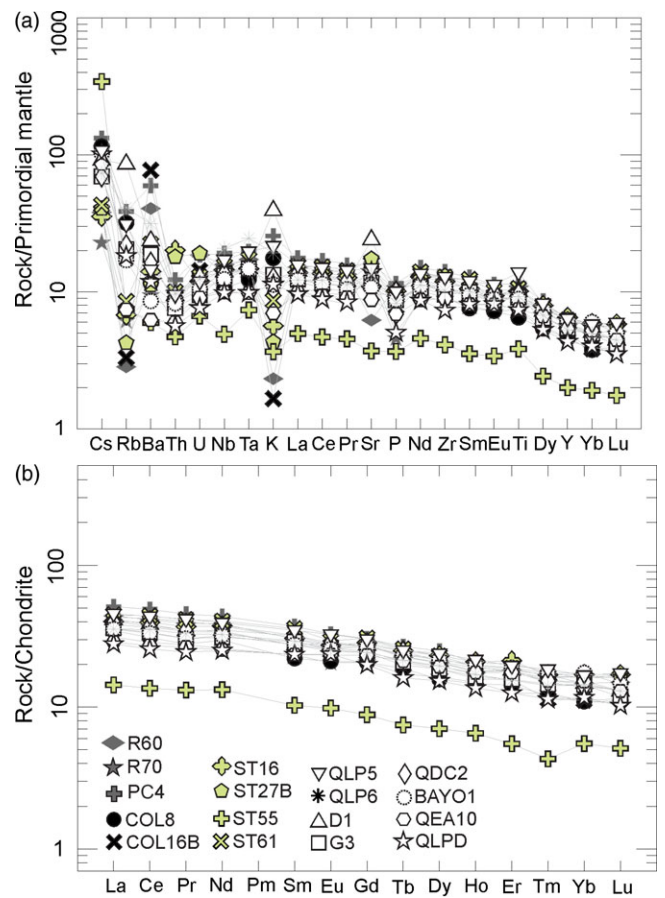


Fig. 10. (Colour online) (a) Primordial mantle-normalized (Sun & McDonough, 1989) incompatible trace-element patterns for the analysed mafic–ultramafic samples. The scattered distribution in Cs, Rb, Ba and K element concentrations is probably due to secondary alteration processes. (b) Chondrite-normalized (Sun & McDonough, 1989) REE patterns. REE contents in analysed rock samples are 10–35 higher than chondrite values. See Figures 1 and 2 for sample location.

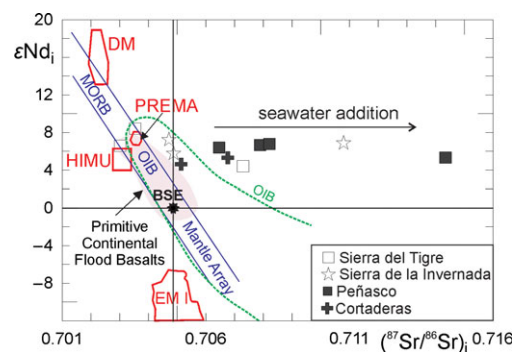


Fig. 11. (Colour online) Initial Nd and Sr isotopic composition diagram. ϵ_{Nd_i} and $(^{87}Sr/^{86}Sr)_i$ are calculated at 418, 454 and 576 Ma according to crystallization ages obtained in basalts (U–Pb on zircon) from the Jagüé-Bonete and Cortaderas areas (Fauqué & Villar, 2003; Davis *et al.* 2000). End-member mantle components after Zindler & Hart (1986) are also shown. DM – depleted mantle; MORB – mid-ocean-ridge basalt; OIB – oceanic-island basalt; PREMA – prevalent mantle; HIMU – high- μ ($\mu = ^{238}U/^{204}Pb$) mantle; BSE – bulk silicate earth; EM1 – enriched mantle. Primitive continental flood basalt field from Condie (2001).

(wehrlite) from the Rodeo and Sierra del Tigre locations present the lowest REE concentrations in comparison to those corresponding to OIB, CFB, E-MORB and N-MORB.

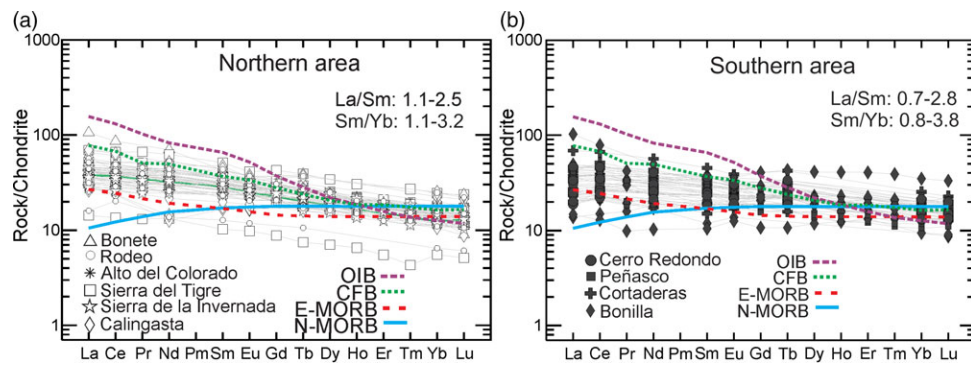


Fig. 12. (Colour online) (a) Chondrite-normalized (Sun & McDonough, 1989) REE patterns from the northern area of the PMUB (La Rioja, Rodeo, Alto del Colorado, Sierra del Tigre, Sierra de la Invernada and Calingasta). Also shown are REE data from Kay *et al.* (1984), Fauqué & Villar (2003), Boedo *et al.* (2013) and González-Menéndez *et al.* (2013). (b) Chondrite-normalized (Sun & McDonough, 1989) REE patterns for samples from the southern PMUB (Cerro Redondo, Peñasco, Cortaderas and Bonilla). Additional REE data are from Cortés & Kay (1994); Cortés *et al.* (1999); Boedo *et al.* (2013); Gregori *et al.* (2013). Ocean island basalts (OIB), continental flood basalts (CFB), E-MORB and N-MORB data (Thompson *et al.* 1983; Sun & McDonough, 1989) also plotted for comparison.

The mafic rocks of the southern sector of the PMUB exhibit a relatively flat HREE trend ranging from slightly depleted to slightly enriched LREE (Fig. 12b). The LREE (La/Sm)_N values range from 0.7 to 2.8, whereas the HREE (Sm/Yb)_N slope is between 0.8 and 3.8. They show lower but also higher LREE and HREE slopes, and a higher REE variation than those for samples from the northern sector of the PMUB, suggesting a transitional N-MORB- to E-MORB-like geochemical signature.

Because the study of different trace elements is useful to identify tectonic setting and crustal contamination input, we used Th/Yb ratios as a proxy for magma–crust interaction or deep crustal recycling indicators (Pearce, 2008). As shown in the Th/Yb versus Ta/Yb diagram of Fig. 13a (Pearce, 1982), the mafic rocks of the PMUB exhibit a MORB–within-plate basalt (WPB) trend, with the majority of the samples lying in the tholeiitic field. Samples from the Bonilla area yield the most variable Th/Yb and Ta/Yb ratios, suggesting the presence of a variety of chemical signatures from N-MORB tholeiitic to E-MORB transitional to alkaline signature. In addition, samples from the Sierra del Tigre and Bonilla areas plotting in the upper part of the MORB–WPB trend may be an indication of not only crustal contamination but also recycled crustal components that imprint similar features to those of arc-related basalts (e.g. Pearce, 2008; Xia & Li, 2019). Similarly, the tectonic discrimination diagram of Cabanis & Thiéblemont (1988) shows that the majority of the analysed mafic rocks have a geochemical signature between N-MORB tholeiitic and E-MORB transitional to alkaline (Fig. 13b). A few samples from the Sierra del Tigre and Bonilla areas lie in the continental alkaline basalts and continental tholeiitic fields, as well as within the arc-related field. When plotted together, samples from the PMUB and mafic lava flows from the Catocin Formation (Neoproterozoic) in the Blue Ridge Mountains of the central Appalachians (Badger & Sinha, 1988, 2004) indicate similar geochemical features (Fig. 13a, b).

5.b. Pressure, temperature and melting depth for magma generation

We estimated pressure (P) and temperature (T) of crystallization in mafic rocks of the northern PMUB using the thermobarometers of Putirka *et al.* (2003) and Putirka (2008). Based on clinopyroxene core and rim compositions (independent of liquid equilibria), we obtained P values between 1.1 and 7.1 kbar (samples QEA10 and KMES9, respectively), with a standard error estimate (SEE) of

± 1.5 kbar (Putirka, 2008). We obtained T values between 1086 and 1199°C (samples KMES10 and KMES 11, respectively) with an SEE of ± 52 to ± 60 °C (Putirka, 2008).

To estimate the P – T conditions based on clinopyroxene–liquid composition, we first test the equilibrium between both phases. In a first approximation for crystal–liquid equilibria, we considered the chemical composition of clinopyroxene cores in our P – T estimation. By comparing observed and predicted values of Fe–Mg exchange, we selected samples with an equilibrium constant K_D (Fe–Mg)^{cpx–liq} in the range of 0.27 ± 0.03 (Putirka, 2008). We obtained P – T conditions of between 1.5 kbar, 1148°C (sample QLP6 from Sierra de la Invernada area) and 6.7 kbar, 1231°C (sample KMES10 from Calingasta area). T values conditions were also estimated using the plagioclase–liquid equilibria thermometer described by Putirka (2008), and we obtained T values between 1123 and 1200°C with an SEE of ± 7 to ± 48 °C (samples QLP6 and BAYO1, respectively, from Sierra de la Invernada area). These values are in good agreement with P – T estimates on clinopyroxene and suggest simultaneous crystallization of clinopyroxene and plagioclase after early crystallization of clinopyroxene crystals. Our results are also consistent with estimations in mafic rocks from the Sierra del Tigre area obtained by González-Menéndez *et al.* (2013) that yielded Grt+Spl pressure conditions and T_c 1215°C. The obtained P – T conditions support the hypothesis of basalt generation at conditions of relatively low pressure in the mantle along the northern sector of the PMUB. Unfortunately, due to the poor representation of mineral chemistry data from the southern PMUB, it is not possible to compare P – T conditions between the northern and southern sectors of the belt. Nevertheless, Cortés & Kay (1994) inferred plagioclase and olivine fractionation at low pressure from minor Eu negative anomalies and low Ni concentration. This would imply similar conditions of crystallization between the northern and southern sectors of the PMUB.

Additional observations based on LREE and HREE systematics show that both the northern and southern PMUB exhibit Sm/Yb ratios of 0.86–2. These ratios suggest that the mafic–ultramafic succession was derived from a mantle source in the spinel–garnet stability field. Since LREE/HREE ratios increase with increasing Moho depth (Mantle & Collins, 2008), we estimate the depth of melting by using Ce/Y ratios for the PMUB samples. Ce/Y ratios ranging over 0.8–1 correspond to an estimated crustal thickness of 20–25 km.

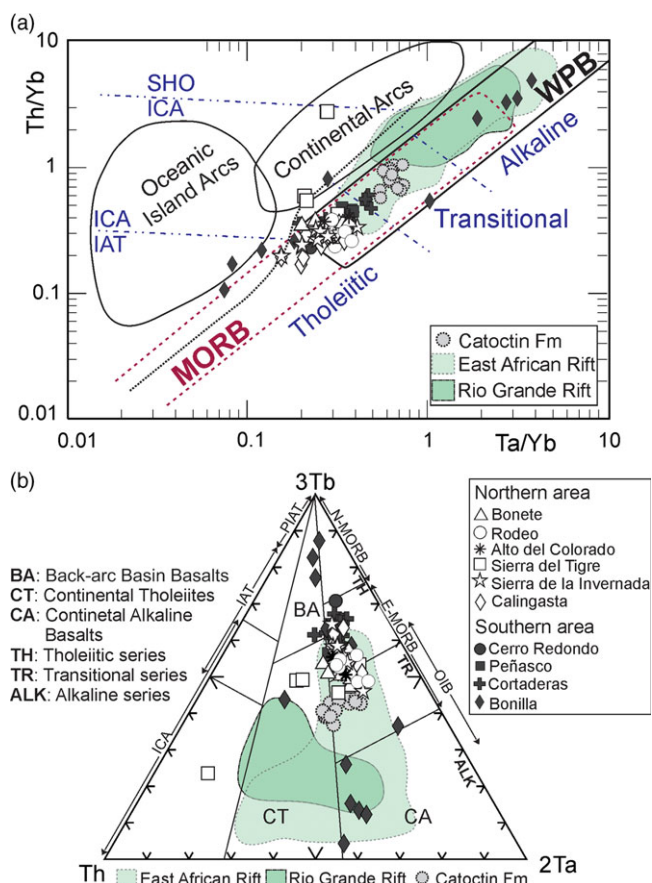


Fig. 13. (Colour online) Tectonic setting of mafic and ultramafic rock samples from the northern and southern PMUB. (a) Th/Yb versus Ta/Tb diagram (after Pearce, 1982). (b) 3Tb (ppm) – Th (ppm) – 2Ta (ppm) diagram (after Cabanis & Thiéblemont, 1988). Samples from Catocctin Formation from Badger & Sinha (2004), representing Neoproterozoic rift-related magmas from eastern North America, are shown for comparison. East African Rift and Rio Grande Rift samples from GEOROC (2020) (<http://georoc.mpch-mainz.gwdg.de/georoc/>), representing modern continental intra-plate settings related to mantle plume activity, are also shown for comparison. N-MORB – normal mid-ocean-ridge basalts; E-MORB – enriched mid-ocean-ridge basalts; WPB – within-plate basalts; PIAT – primitive island-arc tholeiites; OIB – ocean-island basalts; IAT – island-arc tholeiites; ICA – island-arc calc-alkaline basalts; SHO – island-arc shoshonites.

In order to constrain the mantle potential temperature (T_p), we use PRIMELT3 MEGA.xlsm software (Herzberg & Asimow, 2015). Taking into account the estimated low-pressure conditions, and using the major-element composition of the most primitive sample (wehrlite ST55 in Table 2) with Mg no. = 81, we estimated a T_p of 1503°C. A Mg no. of > 70 indicates that sample ST55 represents a direct partial melt of the mantle source. Liquidus temperature calculated in basalts, gabbros and diorite are between 1120 and 1440°C, with the lowest temperature for diorite ST27B (Mg no. 39) and the highest for gabbro COL8 (Mg no. 67) (Table 2).

6. Discussion

6.a. Assessment of crustal contamination and mantle source

Although basaltic magmas are believed to retain reliable geochemical traces of their tectonic setting of origin, using geochemical signatures alone to discriminate between continental intraplate basalts, including continental flood basalts and continental rift basalts, and arc basalts could be misleading (Xia, 2014).

Assimilation of sedimentary material and/or the contamination by continental crust or lithosphere can impart a subduction-like signature (e.g. negative Nb, Ta and Ti anomalies) and lead to the misidentification of contaminated CFB (Ernst *et al.* 2005; Xia, 2014). In this sense, the lack of Nb-Ta and Ti depletion in PMUB argues against subduction components, but ancient crustal recycled materials can provide a crustal or subduction-like signal. In addition, the concentration of incompatible trace elements in contaminated CFB is markedly higher than those of arc-related basalts (Xia & Li, 2019). The scattered distribution in LILEs (such as Cs, Rb, Ba, K and Sr) (Fig. 10a) observed in the studied samples reflects features associated with post-magmatic/hydrothermal alteration. According to Reichow *et al.* (2005), high Ba concentration can be explained by post-emplacment/hydrothermal alteration and/or crustal contamination. Ba concentration observed in our mafic samples ranges over 41.5–539 ppm (Table 2). In addition, low La/Ba ratios (0.02–0.15) versus almost constant La/Nb (0.6–1) would be expected if hydrothermal fluids mobilize Ba and deplete the samples in Rb, K and Sr (Fig. 10a). This observation is consistent with Sr isotope data. The large Sr dispersion observed at relative constant ϵ_{Nd} values (Fig. 11) can be better explained by Rb enrichment and Sr depletion by means of seawater addition (McCulloch *et al.* 1980), rather than the effect of magmatic processes such as crustal contamination and/or subduction processes. Nevertheless, slight crustal contamination processes should not be discarded.

Several studies have shown that the composition of basaltic magmas for a given mantle source depends on two factors: (1) the mantle temperature; and (2) the lithospheric thickness (e.g. McKenzie & O’Nions, 1991; Watson & McKenzie, 1991). Mantle potential temperatures obtained in mafic–ultramafic samples from the PMUB indicate a mantle potential temperature significantly above ambient mantle (ΔT_p of c. 50–100°C), which is estimated as 1280–1400°C (Herzberg *et al.* 2007). This suggests a thermal anomaly that can be related to the presence of a mantle plume involved in the production of the PMUB magmatism. Nd isotope compositions showing the interaction of HIMU and PREMA mantle reservoirs (Fig. 11) are also indicative of mantle plume activity (Condie, 2001). The ΔNb ($\Delta Nb = 1.74 + \log(Nb/Y) - 1.92 \log(Zr/Y)$; Fitton *et al.* 1997) calculated for the PMUB mafic rocks reach values of up to +0.47, indicating that Nb is enriched 4.7 times relative to a ΔNb of 0 for a given Zr/Y (Fitton *et al.* 1997). Zr/Y and Nb/Y systematics suggest the requirement of a component derived from recycled oceanic crust mixed with a depleted mantle component described in tectonic settings with mantle plume activity (Condie, 2001). In particular, a PREMA mantle source (sample ST55 in Fig. 11) may itself represent the melting of a mantle reservoir with intermediate composition between DMM (depleted MORB mantle), BSE, HIMU and EM (enriched mantle) end-member components (Zindler & Hart, 1986). ΔNb positive values, together with Nd isotope composition and REE–HFSE systematics (Figs 11–13) support the hypothesis of a mantle plume influence in the source of the PMUB.

In addition, geochemical features of the mafic rocks from the PMUB were compared with mafic units from two modern continental intra-plate settings, which are definitely related to mantle plume activity: the Rio Grande Rift of western North America and the East African Rift. We observed that mafic rocks from the southern PMUB (e.g. Bonilla, Cortaderas and Peñasco areas) show a relatively good correlation with the Rio Grande and the East African Rift settings (Fig. 13a); in contrast, Th–Tb–Ta concentrations can be compared with samples from the Rio

Grande Rift, with the majority of the PMUB samples plotting in that field (Fig. 13b). This observation supports transitional affinity between MORB and WPB for the PMUB.

The Nd isotopic evolution with time indicates that, at the moment of crystallization of the mafic rocks, the highly positive ϵ_{Nd} values (from +3.4 to +8.4) lie below the depleted mantle curve of DePaolo (1988). This supports the above-mentioned hypothesis that the mafic rocks derive from an enriched mantle source or an old depleted mantle material mixed with a crustal component (Fig. 14). In particular, samples lying over or near the depleted mantle evolution curve exhibit only slight or poor crustal contamination. Nd isotope composition of the studied mafic rocks is comparable with that of Neoproterozoic–Cambrian mafic rocks from the Catoctin Formation in the Blue Ridge Mountains of the central Appalachians, southern Appalachians and the Southern Oklahoma Aulacogen in the current North American Plate (Fullagar *et al.* 1997; Badger *et al.* 2010; Brueseke *et al.* 2016). The Neoproterozoic rift-related magmas from eastern North America have been attributed to the interaction of a plume with the subcontinental lithospheric mantle (Puffer, 2002) or a mantle plume that incorporated an eclogite component from subducted mantle slabs (Badger & Sinha, 2004). It is therefore possible that the mantle source for the PMUB mafic magmatism was derived in part from a Mesoproterozoic–Neoproterozoic basement exposed in the SE Laurentian Grenville Province (Fig. 14). In this context, our $\epsilon_{\text{Nd}}(t)$ values (+3.4 to +8.4, at 418, 454 and 576 Ma), other similar observations ($\epsilon_{\text{Nd}}(t)$ values +6.5 to +7.5 obtained by Davis *et al.* 2000; Kay *et al.* 2005; Martina *et al.* 2014 in the PMUB) and data from the Guarguaraz area in the Argentine Frontal Cordillera (López & Gregori, 2004; López de Azarevich *et al.* 2009) may indicate a common primitive magmatic source with a Grenville affinity. The igneous–sedimentary succession developed on a Grenville-aged crust for the PMUB is suggested by the presence of Mesoproterozoic rocks and equivalent Nd model ages in the Cordón del Portillo and other areas such as the Jagüé–Bonete locality, the Pie de Palo, Umango and Maz ranges, and the San Rafael and Las Matras blocks (e.g. Varela *et al.* 2011). Mesoproterozoic basic rocks of the Sierra de Pie de Palo in the Sierras Pampeanas (Fig. 1; Kay *et al.* 1996) show an Nd isotope evolution trend comparable with our results, suggesting a possible correlation with this region of the Cuyania terrane (Fig. 14).

Nd model ages of the PMUB correlate closely with the age of the Rodinia break-up and opening of the Iapetus Ocean along the Blue Ridge Rift of southeastern Laurentia (572 ± 5 to 564 ± 9 Ma; Aleinikoff *et al.* 1995). In particular, Neoproterozoic–Cambrian mafic rocks from the PMUB and those from the Catoctin Formation and the Southern Oklahoma Aulacogen in North America seem to be contemporaneous and share a similar plume-enriched mantle source or an old recycled enriched Laurentian component (Fullagar *et al.* 1997; Badger *et al.* 2010; Brueseke *et al.* 2016). This similarity, as well as Nd–Hf–Pb similarities between basement rocks from Cuyania and Chilenia (Jacques *et al.* 2020), may support the theory that both terranes derive from Laurentia.

In any case, the availability of more reliable crystallization ages in the framework of previous geological observations is critical to better constrain: (1) the evolution of magmatic events in the Cuyania–Chilenia and Laurentian margin, from the rift-drift phase until final separation; and (2) the rift-related magmatism between the Chilenia and the Cuyania terranes during Neoproterozoic – early Palaeozoic time.

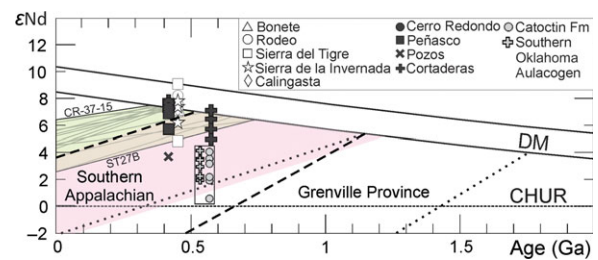


Fig. 14. (Colour online) Nd isotopic evolution diagram for mafic and ultramafic rocks from the PMUB. The green shaded area indicates extreme evolution lines (samples CR 37-15 and ST27B) for analysed samples. Depleted mantle evolution curve model is after DePaolo (1981). CHUR – chondritic uniform reservoir. Dotted lines represent the field for Grenville Province from Lambert *et al.* (1988); Smith *et al.* (1997); Goldberg & Dallmeyer (1997); Fisher *et al.* (2010). Dashed lines indicating the field for southern Appalachian from Fullagar *et al.* (1997). The pink shaded area indicates the field for mafic and ultramafic protoliths from the Pie de Palo basement and Pie de Palo Complex (Kay *et al.* 1996; Rapela *et al.* 2010). Samples from the Catoctin Formation (Badger *et al.* 2010) and from Southern Oklahoma Aulacogen (Brueseke *et al.* 2016) are shown for comparison.

6.b. Tectonic implications

In the context of the Rodinia break-up, the evolution of the SE Laurentian margin began with the opening of the Iapetus Ocean in successive pulses during 750–540 Ma from north to south (from Tennessee and Virginia areas to the Ouachita embayment) (e.g. Thomas *et al.* 2012). Recently, Domeier & Jakob (2020) have proposed that the opening of the Iapetus Ocean involved two ‘Iapetan’ ocean basins: the Palaeo-Iapetus at 700 Ma, and the Neo-Iapetus at 600 Ma. According to that study, in the latter episode the Neo-Iapetus origin led to the detachment of small terranes, the drifting of these towards western Gondwana, the subduction of the Palaeo-Iapetus mid-ocean ridge and the arrival of a mantle plume at *c.* 615 Ma. Lithospheric weakness may derive from a regional extension and intra-continental rifting associated with the Neoproterozoic magmatism (e.g. the Catoctin flood basalts at *c.* 570–565 Ma; Badger & Sinha, 1988; Badger *et al.* 2010).

Comparing those observations with our results for the PMUB, we propose that the magmatism in southern PMUB (with T_{DM} ages of 750–556 Ma) started with the first opening stage of the Iapetus Ocean and continued with the second stage related to the Neo-Iapetus (Domeier & Jakob, 2020) at 600 Ma. Our results show that the T_{DM} estimations of 600–550 Ma fit well with reported magmatism in the central to southern Appalachians. The extending magmatism through Neoproterozoic–Cambrian time evolved as an E-MORB intra-continental rift magmatism to a proto narrow ocean with N-MORB-like magmatism.

The predominant mafic and ultramafic magmatism in the northern PMUB seems to have evolved as an intra-continental rift margin with younger T_{DM} ages (468–416 Ma) and E-MORB geochemical signature.

In our model: (1) the intracontinental extension recorded between the Chilenia and Cuyania terranes in both northern and southern PMUB sectors did not lead to the final separation and opening of an evolved ocean basin; and (2) the E-MORB-like geochemical signature along the PMUB could be more likely described as a plume-distal ridge effect simultaneous to the origin of the incipient Cuyano ocean basin. This agrees with predictions from computational modelling and experimental data supporting the theory that mantle plumes may be laterally zoned up to a length of 1000 km, and may exhibit a compositionally enriched central portion with a more depleted outer region (Jones *et al.* 2016).

Mafic magmatism was probably driven by an extensional large-scale fault dipping to the west in a thinned (*c.* 20–25 km thick) continental crust. High-frequency receiver function (RF) analyses computed in the Andean back-arc region (*c.* 31–32° S) suggest the presence of a W-dipping ancient master fault compressively reactivated between the Chilenia and Cuyania terranes (Ammirati *et al.* 2016; Ariza *et al.* 2018). This major structure recognized in the suture zone between these terranes may affect the whole crust and was probably inverted as reverse faulting, driving to the formation of the Proto-Precordillera during Middle–Late Devonian time (Amos & Rolleri, 1965; Davis *et al.* 1999, 2000; Willner *et al.* 2011) or probably during the Late Devonian – Early Carboniferous interval (e.g. Heredia *et al.* 2012; Giambiagi *et al.* 2014). Under compression, this major structure would have played a role leading the Cuyania basement under the Chilenia basement in a continental collision.

We propose that extensional stresses began south of 32° S in the PMUB and the Argentine Frontal Cordillera mafic–ultramafic belt and continued northwards up to 28° S. The Cuyania terrane may therefore have been partially rifted away from the Chilenia terrane through a probably late Neoproterozoic? large-scale fault and later accreted again during Middle–Late Devonian time (*c.* 390–365 Ma) (Ramos *et al.* 1986; Davis *et al.* 1999, 2000; Willner *et al.* 2011). In this interpretation, the Chilenia terrane is parautochthonous to Cuyania and both are part of a larger block (Dalla Salda *et al.* 1992; Dalziel *et al.* 1994; López & Gregori, 2004).

Although we do not have enough geological and geochronological evidence to state that the complete rift-drift process occurred during the Neoproterozoic – early Palaeozoic evolution between the Cuyania and Chilenia terranes and Laurentian margin, we find evidence from trace-element systematics and Nd isotopic data suggesting that the complex interaction between a mantle plume during Neoproterozoic time and a Grenville Laurentian basement contributed to the source of the studied PMUB magmatism.

7. Conclusions

New geochemical data of basalts, gabbros, leuco-gabbro-norite, diorite and wehrlites from the northern sector of the PMUB yield enriched chondrite-normalized REE trends with low to moderate LREE/HREE ratios and slight negative to positive Eu anomalies. These patterns are compatible with an E-MORB to CFB geochemical signature. Major-element chemistry of clinopyroxene crystals from the analysed rocks also support a tholeiitic affinity. Estimations of *P*–*T* crystallization conditions (1.1–7.1 kbar, 1086–1231°C) suggest that crystallization occurred at low pressures.

The studied mafic rocks have ϵ_{Nd} values between +3.4 and +8.4, which are lower than the depleted mantle. Low to high $^{87}\text{Sr}/^{86}\text{Sr}$ ratios of 0.7030–0.7143 seem to have been controlled by hydrothermal and/or post-emplacement alteration.

The integration of these new data with previous geochemical studies of the PMUB allow us to recognize that the northern sector of the PMUB has REE trends compatible with an E-MORB to CFB signature, whereas the southern sector exhibits a transitional E-MORB to N-MORB-like signature.

The Nd isotopic evolution with time indicates that the PMUB mafic rocks register the influence of an enriched mantle component or an old depleted mantle material mixed with a crustal component. In particular, samples lying over or near the depleted mantle evolution curve exhibit only slight crustal contamination.

REE trends and HFSE concentrations (e.g. positive ΔNb), together with the estimation of a high potential mantle temperature ($T_{\text{p}} = 1503^\circ\text{C}$; ΔT_{p} *c.* 50–100°C above ambient mantle), point to the effect of a distal rising plume as a possible mechanism for the generation of the E-MORB/CFB studied rocks.

Depleted mantle Nd model ages (T_{DM}) suggest that magmatic activity started in the southern PMUB during middle–late Neoproterozoic time (750–557 Ma) and continued N-wards during late Cambrian – Early Devonian time (490–416 Ma) over an extended margin. Our results suggest that the Neoproterozoic evolution of the PMUB is comparable to that of the assumed conjugated Laurentian margin. The early Neoproterozoic E-MORB magmatic activity can be linked to the effect of a distal mantle plume during the Iapetus Ocean opening. In particular, estimated T_{DM} of 600–550 Ma could be linked to the plume-related magmatic activity in the central and southern Appalachians (e.g. Catoctin Formation), giving support to a contemporaneous origin and a similar plume-enriched mantle source.

Acknowledgements. This contribution has been funded by the Consejo Nacional de Investigaciones Científicas y Técnicas (CONICET-PIP 0072) and Ministerio de Ciencia, Tecnología e Innovación Productiva de Argentina (FONCyT-PICT2016-0046). The authors thank the members of staff of the Laboratório de Geoquímica Isotópica e Geocronologia of the Universidade de Brasília (Brazil) for making available their analytical facilities. We also thank Dr Fernando Colombo and Dr Alina Guereschi for their assistance at the Laboratorio de Microscopía Electrónica y Análisis de Rayos X (LAMARX) of the Universidad Nacional de Córdoba (Argentina). We are also grateful to the editor Dr Kathryn Goodenough, as well as Dr Veronica Oliveros and an anonymous reviewer, for their very helpful comments that significantly improved an earlier version of the manuscript.

Supplementary material. To view supplementary material for this article, please visit <https://doi.org/10.1017/S0016756821000303>

References

- Aleikoff JN, Zartman RE, Walter M, Rankin DW, Lyttle PT and Burton WC (1995) U–Pb ages of metarhyolites of the Catoctin and Mount Rogers Formations, central and southern Appalachians: evidence for two pulses of Iapetan rifting. *American Journal of Science* **295**, 428–54.
- Ammirati JB, Pérez Luján S, Alvarado P, Beck S, Rocher S and Zandt G (2016) High-resolution images above the Pampean flat slab of Argentina (31–32°S) from local receiver functions: implications on regional tectonics. *Earth and Planetary Science Letters* **450**, 29–39.
- Amos AJ and Rolleri EO (1965) El Carbónico marino en el Valle Calingasta–Uspallata (San Juan y Mendoza). *Boletín de Informaciones Petroleras* **368**, 1–23.
- Ariza JP, Boedo FL, Sánchez MA, Christiansen R, Pérez Luján S, Vujovich G and Martínez P (2018) Structural setting of the Chanic orogen (Upper Devonian) at central-western Argentina from remote sensing and aeromagnetic data. Implications in the evolution of the proto-Pacific margin of Gondwana. *Journal of South American Earth Sciences* **88**, 352–66.
- Astini RA, Benedetto JL and Vaccari NE (1995) The Early Paleozoic evolution of the Argentine Precordillera as a Laurentian rifted, drifted and collided terrane: a geodynamic model. *Geological Society of America Bulletin* **107**, 253–73.
- Badger RL, Ashley KT, Cousens BL, Tollo RP, Bartholomew MJ, Hibbard JP and Karabinos PM (2010) Stratigraphy and geochemistry of the Catoctin volcanics: implications for mantle evolution during the breakup of Rodinia. In *From Rodinia to Pangea: the Lithotectonic Record of the Appalachian Region* (RP Tollo, MJ Bartholomew, JP Hibbard and PM Karabinos), pp. 397–415. Boulder: Geological Society of America, Memoir no. **206**.
- Badger RL and Sinha AK (1988) Age and Sr isotopic signature of the Catoctin volcanic province: implications for subcrustal mantle evolution. *Geology* **16**, 692–95.

- Badger RL** and **Sinha AK** (2004) Geochemical stratigraphy and petrogenesis of the Catoctin volcanic province, central Appalachians. In *Proterozoic Tectonic Evolution of the Grenville Orogen in North America* (eds RP Tollo, J McLelland, L Corriveau and MJ Bartholomew), pp. 435–58. Boulder: Geological Society of America, Memoir no. 197.
- Baldis BA**, **Beresi M**, **Bordonaro O** and **Vaca A** (1982) Síntesis evolutiva de la Precordillera Argentina. *V Congreso Latinoamericano de Geología, Actas 4*, 399–445. Buenos Aires, Argentina.
- Basilici G**, **Cutolo A**, **Gomes Borges JP**, **Henrique A** and **Moretti PA** (2005) Ordovician storm-dominated basin and the evolution of the western Gondwana margin (Portezuelo del Tontal, Sierra de la Invernada and Yerba Loca formations, Argentine Precordillera). In *Gondwana 12. "Geological and Biological Heritage of Gondwana"* (eds RJ Pankhurst and GD Veiga). Mendoza: Academia Nacional de Ciencias, Abstracts, 64.
- Beccaluva L**, **Macciotta G**, **Piccardo GB** and **Zeda O** (1989) Clinopyroxene composition of ophiolitic basalts as petrogenetic indicator. In *Ophiolites and Lithosphere of Marginal Seas* (ed. L. Beccaluva). *Chemical Geology 77*, 165–82.
- Boedo FL**, **Luján SP**, **Naipauer M**, **Vujovich GI**, **Pimentel MM**, **Ariza JP** and **Barredo SP** (2020) The late Neoproterozoic-early Paleozoic basin of the western Argentine Precordillera: insights from zircon U-Pb geochronology. *Journal of South American Earth Sciences 102*, 102669.
- Boedo FL**, **Vujovich GI**, **Kay SM**, **Ariza JP** and **Pérez Luján SB** (2013) The E-MORB like geochemical features of the Early Paleozoic mafic-ultramafic belt of the Cuyania terrane, western Argentina. *Journal of South American Earth Sciences 48*, 73–84.
- Boedo FL**, **Willner AP**, **Vujovich GI** and **Massonne HJ** (2016) High-pressure/low-temperature metamorphism in the collision zone between the Chilenia and Cuyania microcontinents (western Precordillera, Argentina). *Journal of South American Earth Sciences 72*, 227–40.
- Borrello AV** (1969) *Los geosinclinales de la Argentina*. In *Anales XIV, Dirección Nacional de Geología y Minería*. Argentina: Buenos Aires, 188 p.
- Bosworth W**, **Stockli DF** and **Helgeson DE** (2015) Integrated outcrop, 3D seismic, and geochronologic interpretation of Red Sea dike-related deformation in the Western Desert, Egypt—the role of the 23 Ma Cairo “mini-plume”. *Journal of African Earth Sciences 109*, 107–19.
- Brodtkorb MK**, **Herrmann C**, **Pezzutti N**, **Leal P**, **González MP** and **Meissl E** (2015) Mineralización de sulfuros en las ofiolitas Famatinianas y rocas asociadas, Calingasta, Precordillera de San Juan. *Revista de la Asociación Geológica Argentina 72*, 182–94.
- Brueske ME**, **Hobbs JM**, **Bulen CL**, **Mertzman SA**, **Puckett RE**, **Walker JD** and **Feldman J** (2016) Cambrian intermediate-mafic magmatism along the Laurentian margin: evidence for flood basalt volcanism from well cuttings in the Southern Oklahoma Aulacogen (USA). *Lithos 260*, 164–77.
- Cabanis B** and **Thiéblemont D** (1988) La discrimination des tholeiites continentales et des basaltes arriere-arc; proposition d'un nouveau diagramme, le triangle Th-3xTb-2xTa. *Bulletin de la Société Géologique de France 4*, 927–35.
- Casquet C**, **Pankhurst RJ**, **Rapela CW**, **Galindo C**, **Fanning CM**, **Chiaradia M**, **Baldo E**, **González-Casado JM** and **Dahlquist JA** (2008) The Mesoproterozoic Maz terrane in the Western Sierras Pampeanas, Argentina, equivalent to the Arequipa–Antofalla block of southern Peru? Implications for West Gondwana margin evolution. *Gondwana Research, 13*, 163–75.
- Condie KC** (2001) *Mantle Plumes and their Record in Earth History*. Cambridge: Cambridge University Press, 306 p.
- Cortezi C**, **Furque G** and **Paulicevic R** (1982) Estudio petrológico de las lavas en almohadilla del Katiano inferior a medio de la zona de Rodeo, Departamento Iglesia, Provincia de San Juan, República Argentina. In *V Congreso Latinoamericano de Geología, 17–22 October 1982*, Buenos Aires, Actas 2, 161–72. Servicio Geológico Nacional.
- Cortés JM** (1992) Lavas almohadilladas en el Grupo Ciénaga del Medio del extremo noroccidental de la Precordillera mendocina. *Revista Asociación Geológica Argentina 47*, 115–17.
- Cortés JM**, **González Bonorino G**, **Koukharsky ML**, **Brodtkorb A**, **Pereyra F** (1999) Hoja Geológica 3369-03 Yalguaraz, Mendoza (versión preliminar), Escala 1:100, Carta Geológica de la República Argentina. Buenos Aires: Servicio Geológico Minero Argentino.
- Cortés JM** and **Kay S** (1994) Una dorsal oceánica como origen de las lavas almohadilladas del Grupo Ciénaga del Medio (Silúrico-Devónico) de la Precordillera de Mendoza, Argentina. In *7º Congreso Geológico Chileno, 17–21 October 1994*, Concepción, Chile. Actas 2, 1005–9. Universidad de Concepción.
- Cucchi RJ** (1971) Edades radimétricas y correlación de metamorfitas de la Precordillera de San Juan - Mendoza. República Argentina. *Revista de la Asociación Geológica Argentina 26*, 503–515.
- Dalla Salda L**, **Cingolani CA** and **Varela R** (1992) Early Paleozoic orogenic belt of the Andes in southwestern South America. Results of Laurentian-Gondwana collision? *Geology 20*, 617–21.
- Dalziel IWD**, **Dalla Salda LH** and **Gahagan LM** (1994) Paleozoic Laurentia-Gondwana interaction and the origin of the Appalachian Andean mountain system. *Geological Society of America Bulletin 106*, 243–52.
- Davis J**, **Roeske S**, **McClelland W** and **Kay S** (2000) Mafic and ultramafic crustal fragments of the southwestern Precordillera terrane and their bearing on tectonic models of the early Paleozoic in western Argentina. *Geology 28*, 171–74.
- Davis J**, **Roeske S**, **McClelland W** and **Snee L** (1999) Closing an ocean between the Precordillera terrane and Chilenia: early Devonian ophiolite emplacement and deformation in the southwest Precordillera. In *Laurentia-Gondwana Connections before Pangea* (eds VA Ramos and JD Keppie), pp. 115–38. Boulder: Geological Society of America, Special publication no. 336.
- De Min A**, **Piccirillo EM**, **Marzoli A**, **Bellieni G**, **Renne PR**, **Ernesto M** and **Marques LS** (2003) The Central Atlantic Magmatic Province (CAMP) in Brazil: petrology, geochemistry, 40Ar/39Ar ages, paleomagnetism and geodynamic implications. In *The Central Atlantic Magmatic Province: Insights from Fragments of Pangea* (eds W Hames, JG Mchone, P Renne and C Ruppel), pp. 91–128. Washington, DC: American Geophysical Union, Geophysical Monograph no. 136.
- DePaolo DJ** (1981) Neodymium isotopes in the Colorado Front Range and crust–mantle evolution in the Proterozoic. *Nature 291*, 193–96.
- DePaolo DJ** (1988) *Neodymium Isotope Geochemistry: An Introduction*. Berlin, Heidelberg, New York, London, Paris, Tokyo: Springer-Verlag, Minerals and Rocks Series no. 20, xi + 187 p.
- DePaolo DJ** and **Wasserburg GJ** (1976) Inferences about magma sources and mantle structure from variations of 143Nd/144Nd. *Geophysical Research Letters 3*, 743–46.
- Dilek Y** and **Furnes H** (2011) Ophiolite genesis and global tectonics: geochemical and tectonic fingerprinting of ancient oceanic lithosphere. *Geological Society of America Bulletin 123*, 387–411.
- Domeier M** and **Jakob J** (2020) Iapetan Oceans: an analog of Tethys? *Geology 48*, 929–33.
- Donnelly KE**, **Goldstein SL**, **Langmuir CH** and **Spiegelman M** (2004) Origin of enriched ocean ridge basalts and implications for mantle dynamics. *Earth and Planetary Science Letters 226*, 347–66.
- Ernst RE**, **Buchan KL** and **Campbell IH** (2005) Frontiers in large igneous province research. *Lithos 79*, 271–97.
- Fauqué L** and **Villar L** (2003) Reinterpretación estratigráfica y petrología de la Formación Chuscho, Precordillera de La Rioja. *Revista de la Asociación Geológica Argentina 58*, 218–32.
- Finney S** (2007) The parautochthonous Gondwanan origin of the Cuyania (greater Precordillera) terrane of Argentina: a re-evaluation of evidence used to support an allochthonous Laurentian origin. *Geologica Acta: An International Earth Science Journal 5*, 127–58.
- Fisher CM**, **Loewy SL**, **Miller CF**, **Berquist P**, **Van Schmus WR**, **Hatcher RD Jr**, **Wooden JL** and **Fullagar PD** (2010) Whole-rock Pb and Sm-Nd isotopic constraints on the growth of southeastern Laurentia during Grenvillian orogenesis. *Geological Society of America Bulletin 122*, 1646–59.
- Fitton JG**, **Saunders AD**, **Norry MJ**, **Hardarson BS** and **Taylor RN** (1997) Thermal and chemical structure of the Iceland plume. *Earth and Planetary Science Letters 153*, 197–208.
- Fullagar PD**, **Goldberg SA** and **Butler JR** (1997) Nd and Sr isotopic characterization of crystalline rocks from the southern Appalachian Piedmont and Blue Ridge, North and South Carolina. In *The Nature of Magmatism in the Appalachian Orogen* (eds AK Sinha, JB Whalen and JP Hogan), pp. 165–79. Boulder: Geological Society of America, Memoir no. 191.

- Furque G** (1983) Descripción Geológica de la Hoja 19c - Ciénaga de Gualilán. Carta Geológico-Económica de la República Argentina. Escala 1:200.000. Provincia de San Juan. Boletín 193, 126 p. Buenos Aires, Servicio Geológico Nacional.
- Gargiulo MF, Bjerg EA, Mogessie A** (2011) Caracterización y evolución metamórfica de las rocas ultramáficas de la Faja del río de las Tunas, Cordillera Frontal de Mendoza. *Revista Asociación Geológica Argentina* **68**, 571–93.
- Giambiagi L, Mescua J, Heredia N, Fariás P, García Sansegundo J, Fernandez C, Stier S, Pérez D, Bechis F, Moreiras SM and Lossada A** (2014) Reactivation of Paleozoic structures during Cenozoic deformation in the Cordón del Plata and Southern Precordillera ranges (Mendoza, Argentina). *Journal of Iberian Geology* **40**, 309–20.
- Gioia SMCL and Pimentel MM** (2000) The Sm-Nd isotopic method in the geochronology laboratory of the University of Brasília. *Anais da Academia Brasileira de Ciências* **72**, 219–45.
- Gomes JPB, Basilici G, Cutolo AA, Henrique A and Moretti PA Jr** (2005) The importance of storm-gravitational combined flows on the construction of sandstone reservoirs in siliciclastic shelves: analogous in Portezuelo del Tontal and Sierra de la Invernada Formations (middle-upper Ordovician, Precordillera Argentina). In *Gondwana 12 "Geological and Biological Heritage of Gondwana"*, Mendoza, Academia Nacional de Ciencias, Abstracts, p. 174.
- González-Menéndez L, Gallastegui G, Cuesta A, Heredia N and Rubio-Ordóñez A** (2013) Petrogenesis of Early Paleozoic basalts and gabbros in the western Cuyania terrane: constraints on the tectonic setting of the southwestern Gondwana margin (Sierra del Tigre, Andean Argentine Precordillera). *Gondwana Research* **24**, 359–76.
- Green DH and Ringwood AE** (1967) The stability field of aluminous pyroxene peridotite and garnet peridotite and their relevance in upper mantle structure. *Earth and Planetary Science Letters* **3**, 151–60.
- Gregori DA, Martínez JC and Benedini L** (2013) The Gondwana-South America Iapetus margin evolution as recorded by Lower Paleozoic units of western Precordillera, Argentina: the Bonilla Complex, Uspallata. Instituto Superior de Correlación Geológica. Serie Correlación Geológica no. 29, 21–80. San Miguel de Tucumán.
- Goldberg SA and Dallmeyer RD** (1997) Chronology of Paleozoic metamorphism and deformation in the Blue Ridge thrust complex, North Carolina and Tennessee. *American Journal of Science* **297**, 488–526.
- Haller MJ, Ramos VA** (1984) Las ofiolitas famintinianas (Eopaleozoico) de las provincias de San Juan y Mendoza. In *9º Congreso Geológico Argentino*, 5–9 November 1984, San Carlos de Bariloche, Argentina. Actas 3, 66–83. Asociación Geológica Argentina.
- Heredia N, Fariás P, García Sansegundo J and Giambiagi L** (2012) The basement of the Andean Frontal Cordillera in the Cordón del Plata (Mendoza, Argentina): geodynamic evolution. *Andean Geology* **39**, 242–57, <https://doi.org/10.5027/andgeoV39n2-a03>.
- Herzberg C and Asimow PD** (2015) PRIMELT 3 MEGA. XLSM software for primary magma calculation: peridotite primary magma MgO contents from the liquidus to the solidus. *Geochemistry, Geophysics, Geosystems* **16**, 563–78.
- Herzberg C, Asimow PD, Arndt N, Niu Y, Leshner CM, Fitton JG and Saunders AD** (2007) Temperatures in ambient mantle and plumes: constraints from basalts, picrites, and komatiites. *Geochemistry, Geophysics, Geosystems* **8**(2), <https://doi.org/10.1029/2006GC001390>.
- Jacques G, Hauff F, Hoernle K, Jung S, Kay SM, Garbe-Schönberg D and Bindeman I** (2020) Sr-Nd-Pb-Hf-O isotopic constraints on the Neoproterozoic to Miocene upper and mid crust in central Chile and western Argentina and trench sediments (33°–35° S). *Journal of South American Earth Sciences* **104**, 102879.
- Jones TD, Davies DR, Campbell IH, Wilson CR and Kramer SC** (2016) Do mantle plumes preserve the heterogeneous structure of their deep-mantle source? *Earth and Planetary Science Letters* **434**, 10–17.
- Kay S, Ramos V and Kay R** (1984) Elementos mayoritarios y trazas de las vulcanitas ordovícicas de la Precordillera occidental; basaltos de rift oceánico temprano (?) próximo al margen continental. In *9º Congreso Geológico Argentino*, 5–9 November 1984, San Carlos de Bariloche, Argentina. Actas 2, 48–65. Asociación Geológica Argentina.
- Kay SM, Godoy E and Kurtz A** (2005) Episodic arc migration, crustal thickening, subduction erosion, and magmatism in the south-central Andes. *Geological Society of America Bulletin* **117**, 67–88.
- Kay SM, Orrell S and Abruzzi JM** (1996) Zircon and whole-rock Nd–Pb isotopic evidence for a Grenville age and Laurentian origin for the basement of the Precordillera in Argentina. *Journal of Geology* **104**, 637–48.
- Lambert DD, Unruh DM and Gilbert MC** (1988) Rb–Sr and Sm–Nd isotopic study of the Glen Mountains layered complex: initiation of rifting within the southern Oklahoma aulacogen. *Geology* **16**, 13–17.
- Le Bas MJ** (1962) The role of aluminium in igneous clinopyroxenes with relation to their parentage. *American Journal of Science* **260**, 267–88.
- Leterrier J, Maury RC, Thonon P, Girard D and Marchal M** (1982) Clinopyroxene composition as a method of identification of the magmatic affinities of paleo-volcanic series. *Earth and Planetary Science Letters* **59**, 139–154.
- Leveratto MA** (1968) Geología de la zona al oeste de Ullum y Zonda, borde oriental de la Precordillera de San Juan, eruptividad subvolcánica y estructura. *Revista de la Asociación Geológica Argentina* **23**, 129–57.
- Lin J, Liu Y, Yang Y and Hu Z** (2016) Calibration and correction of LA-ICP-MS and LA-MC-ICP-MS analyses for element contents and isotopic ratios. *Solid Earth Sciences* **1**, 5–27.
- López VL and Gregori DA** (2004) Provenance and evolution of the Guarguaraz Complex, Cordillera Frontal, Argentina. *Gondwana Research* **7**, 1197–208.
- López de Azarevich VLL, Escayola M, Azarevich MB, Pimentel MM and Tassinari C** (2009) The Guarguaraz Complex and the Neoproterozoic–Cambrian evolution of southwestern Gondwana: geochemical signatures and geochronological constraints. *Journal of South American Earth Sciences* **28**, 333–44.
- Lugmair GW and Marti K** (1978) Lunar initial ¹⁴³Nd/¹⁴⁴Nd: differential evolution line of the lunar crust and mantle. *Earth and Planetary Science Letters* **39**, 349–57.
- MacDougall JD** (ed.) (1988) *Continental Flood Basalts* (Vol. 3). New York: Springer Science & Business Media.
- Mantle GW and Collins WJ** (2008) Quantifying crustal thickness variations in evolving orogens: correlation between arc basalt composition and Moho depth. *Geology* **36**, 87–90.
- Martina F, Astini RA and Pimentel MM** (2014) Sr–Nd isotope data of basement rocks from the northernmost Argentine Precordillera and its implications for the early Paleozoic evolution of SW Gondwana margin. *Journal of South American Earth Sciences* **56**, 20–29.
- Massonne H-J and Calderón M** (2008) P–T evolution of metapelites from the Guarguaraz Complex, Argentina: evidence for Devonian crustal thickening close to the western Gondwana margin. *Revista Geológica de Chile* **35**, 215–31.
- McCulloch MT, Gregory RT, Wasserburg GJ and Taylor HP Jr** (1980) A neodymium, strontium, and oxygen isotopic study of the Cretaceous Samail ophiolite and implications for the petrogenesis and seawater-hydrothermal alteration of oceanic crust. *Earth and Planetary Science Letters* **46**, 201–11.
- McKenzie DAN and O'Nions RK** (1991) Partial melt distributions from inversion of rare earth element concentrations. *Journal of Petrology* **32**, 1021–91.
- Moretti PA** (2009) Análise de Fácies e Modelo Paleodeposicional da Plataforma Siliciclástica Ordovíciana da Pré-Cordilheira Argentina. Subcomissão de Pós-graduação em Ciências e Engenharia de petróleo, Faculdade de Engenharia Mecânica e Instituto de Geociências, Universidade Estadual de Campinas, 126 p. São Paulo, Brasil.
- Morimoto N** (1988) Nomenclature of pyroxenes. *Mineralogy and Petrology* **39**, 55–76.
- Ortega G, Albanesi GL, Banchig AL and Peralta GL** (2008) High resolution conodont-graptolite biostratigraphy in the Middle-Upper Ordovician of the Sierra de la Invernada Formation (Central Precordillera, Argentina). *Geológica Acta* **2**, 161–80.
- Pearce JA** (1982) Trace element characteristics of lavas from destructive plate boundaries. *Andesites* **8**, 525–48.
- Pearce JA** (2008) Geochemical fingerprinting of oceanic basalts with applications to ophiolite classification and the search for Archean oceanic crust. *Lithos* **100**, 14–48, <https://doi.org/10.1016/j.lithos.2007.06.016>.
- Puffer JH** (2002) A late Neoproterozoic eastern Laurentian superplume: location, size, chemical composition, and environmental impact. *American Journal of Science* **302**, 1–27.

- Putirka KD** (2008) Thermometers and barometers for volcanic systems. *Reviews in Mineralogy and Geochemistry* **69**, 61–120.
- Putirka K, Ryerson FJ** and Mikaelian H (2003) New igneous thermobarometers for mafic and evolved lava compositions, based on clinopyroxene + liquid equilibria. *American Mineralogist* **88**, 1542–54.
- Ramos VA, Dallmeyer D** and Vujovich G (1998) Time constraints on the Early Paleozoic docking of the Precordillera, Central Argentina. In *The Proto-Andean Margin of Gondwana* (eds R Pankhurst and CW Rapela), pp. 143–58. Geological Society of London, Special Publication no. 142.
- Ramos VA, Jordan TE, Allmendinger RW, Mpodozis C, Kay SM, Cortés M** and Palma M (1986) Paleozoic terranes of the central Argentine-Chilean Andes. *Tectonics* **5**, 855–80.
- Rapela CW, Pankhurst RJ, Casquet C, Baldo E, Galindo C, Fanning CM** and Dahlquist JM (2010) The Western Sierras Pampeanas: protracted Grenvillite history (1330–1030 Ma) of intra-oceanic arcs, subduction–accretion at continental-edge and AMCG intraplate magmatism. *Journal of South American Earth Sciences* **29**, 105–27.
- Reichow MK, Saunders AD, White RV, Al'Mukhamedov AI** and Medvedev AY (2005) Geochemistry and petrogenesis of basalts from the West Siberian Basin: an extension of the Permo-Triassic Siberian Traps, Russia. *Lithos* **79**, 425–52.
- Robinson D, Bevins R** and Rubinstein N (2005) Subgreenschists facies metamorphism of metabasites from Precordillera of western Argentina; constraints on the later stages of accretion onto Gondwana. *European Journal of Mineralogy* **17**, 441–52.
- Ross PS** and Bédard JH (2009) Magmatic affinity of modern and ancient sub-alkaline volcanic rocks determined from trace-element discriminant diagrams. *Canadian Journal of Earth Sciences* **46**, 823–39.
- Rubinstein CV** and Steemans P (2007) New palynological data from the Devonian Villavicencio Formation, Precordillera of Mendoza, Argentina. *Ameghiniana* **44**, 3–9.
- Rubinstein N, Bevins R, Robinson D** and Morrello O (1997) Very low grade metamorphism in the Alcaparrosa Formation, Western Precordillera, Argentina. In *10° Congreso Latinoamericano de Geología y 6° Congreso Nacional de Geología Económica*, Buenos Aires, Actas 2, pp. 226–29.
- Shervais JW** (1982) Ti–V plots and the petrogenesis of modern and ophiolitic lavas. *Earth and Planetary Science Letters* **59**, 101–18.
- Smith TE, Holm PE, Denisson NM** and Harris MJ (1997) Crustal assimilation in the Burnt Lake metavolcanics, Grenville Province, southeastern Ontario, and its tectonic significance. *Canadian Journal of Earth Science* **34**, 1272–85.
- Sun S** and McDonough W (1989) Chemical and isotopic systematics of oceanic basalts: implications for mantle composition and processes. In *Magmatism in the Ocean Basins* (eds AD Saunders and MJ Norry), pp. 313–45. Geological Society of London, Special Publication no. 42.
- Thomas WA** and Astini RA (2003) Ordovician accretion of the Argentine Precordillera terrane to Gondwana: a review. *Journal of South American Earth Sciences* **16**, 67–79.
- Thomas WA, Tucker RD, Astini RA** and Denison RE (2012) Ages of pre-rift basement and synrift rocks along the conjugate rift and transform margins of the Argentine Precordillera and Laurentia. *Geosphere* **8**, 1366–83, <https://doi.org/10.1130/GES00800.1>.
- Thompson RN, Morrison MA, Dickin AP** and Hendry GL (1983) Continental flood basalts Arachnids rule OK? In *Continental Basalts and Mantle Xenoliths* (CJ Hawkesworth and MJ Norry), pp. 158–85. Cambridge, MA: Shiva Publications.
- Varela R, Basei MAS, González PD, Sato AM, Naipauer M, Campos Neto M, Cingolani CA** and Meira VT (2011) Accretion of Grenvillian terranes to the southwestern border of the Río de la Plata craton, western Argentina. *International Journal of Earth Sciences* **100**, 243–72.
- Watson S** and McKenzie DAN (1991) Melt generation by plumes: a study of Hawaiian volcanism. *Journal of Petrology* **32**, 501–37.
- Whitney D** and Evans B (2010) Abbreviations for names of rock-forming minerals. *American Mineralogist* **95**, 185–87.
- Willner AP, Gerdes A, Massonne HJ, Schmidt A, Sudo M, Thomson SN** and Vujovich G (2011) The geodynamics of collision of a microplate (Chilenia) in Devonian times deduced by the pressure–temperature–time evolution within part of a collisional belt (Guarguaraz Complex, W-Argentina). *Contributions to Mineralogy and Petrology* **162**, 303–27.
- Winchester JA** and Floyd PA (1977) Geochemical discrimination of different magma series and their differentiation products using immobile elements. *Chemical Geology* **20**, 325–43.
- Woodhead J, Eggins S** and Gamble J (1993) High field strength and transition element systematics in island arc and back-arc basin basalts: evidence for multi-phase melt extraction and a depleted mantle wedge. *Earth and Planetary Science Letters* **114**, 491–504.
- Workman RK** and Hart SR (2005) Major and trace element composition of the depleted MORB mantle (DMM). *Earth and Planetary Science Letters* **231**, 53–72.
- Xia L** and Li X (2019) Basalt geochemistry as a diagnostic indicator of tectonic setting. *Gondwana Research* **65**, 43–67.
- Xia LQ** (2014) The geochemical criteria to distinguish continental basalts from arc related ones. *Earth-Science Reviews* **139**, 195–212.
- Zindler A** and Hart S (1986) Chemical geodynamics. *Annual Review of Earth and Planetary Sciences* **14**, 493–571.